communications materials

A Nature Portfolio journal

Review article

https://doi.org/10.1038/s43246-025-00801-7

Covalent organic framework-based cathodes for beyond lithium-ion batteries

Suleman Suleman[1,3], Xiaolong Cheng[1,3], Muhua Gu[1] & Yoonseob Kim[1,2]

Covalent organic frameworks (COFs) are revolutionizing cathode materials for beyond-lithium-ion batteries, leveraging their tunable porosity, modular architecture, and redox-active sites to overcome challenges in the storing alkali metal ions (Na^+ and K^+) and high-valent metal ions (Zn^{2+}, Ca^{2+}, Al^{3+}, Mg^{2+}, etc.) for electrochemical energy storage. Their unique crystal structure, molecular designability, and storage mechanism enable high specific capacity, low diffusion energy barrier, and structural stability when storing large-radius charge carriers. This review highlights recent advancements in COFs for applications beyond lithium-ion batteries, emphasizing performance optimization methodologies for next-generation cathode materials.

Beyond lithium-ion batteries

Pursuing sustainable energy storage systems has become increasingly crucial due to the ever-increasing energy demand and global climate change. Rechargeable lithium (Li)-ion batteries (LIBs) have proven essential in human society and are extensively used in portable electronics, high-power electric vehicles, smart grids, etc[1–3]. Therefore, significant research efforts have focused on improving LIBs performance to meet the energy storage system requirements of diverse application scenarios. In recent years, the rapid expansion of electric vehicles has driven a continuous surge in lithium salt prices, primarily attributed to the low abundance of lithium in the Earth's crust and its concentration in politically sensitive and geographically remote regions[4]. It can be anticipated that the cost of Li salts will become a critical factor limiting the development of LIBs for future large-scale energy storage. To tackle this challenge, beyond Li-ion battery technologies have garnered significant attention as promising alternatives for next-generation energy storage systems. Owing to the similar electrochemical properties of sodium (Na) and potassium (K) with Li and a prominent abundance of elements reservation, Na-ion batteries (SIBs) and K-ion batteries (PIBs) have drawn intensive attention and have been considered two of the most promising next-generation battery systems. Meanwhile, researchers are also increasingly focusing on novel batteries known as high-valent metal ion batteries (HMIBs), which include zinc (Zn) ion batteries (ZIBs), calcium (Ca) ion batteries (CIBs), aluminum (Al) ion batteries (AIBs), and magnesium (Mg) ion batteries (MIBs). These new-type batteries are all based on metal elements with abundant reserve in the Earth's crust and lower reactivity in air, which are promising to deliver high energy density owing to multi-electron redox reaction mechanisms.

Challenges in fabricating cathodes beyond Li-ion batteries

Beyond LIBs share a rocking-chair working mechanism and structural similarities with traditional LIBs, consisting primarily of cathodes, anodes, and electrolytes, etc. Among these components, the choice of cathode material plays a vital role in determining the sustainable and cost-effective energy storage of the battery system. Therefore, to develop these battery systems, various types of cathode materials have been explored, including layered transition metal oxides[5,6], polyanionic compounds[7,8], Prussian blue analogs[9,10], and organic materials[11,12]. However, inorganic cathode materials usually face significant challenges when storing larger cations, such as Na^+ and K^+, including sluggish diffusion kinetics and severe structural degradation[6]. These challenges become even more severe regarding high-valent metal ions, such as Zn^{2+}, Ca^{2+}, Al^{3+}, $AlCl^{2+}$, and $AlCl_2^+$, etc., with larger radii, primarily due to the strong Coulombic interactions between multivalent cations and the negatively charged host lattice. These interactions significantly increase the ionic migration energy barrier, leading to sluggish electrode reaction kinetics[13,14]. More importantly, charge carriers in the electrolyte typically interact with solvent molecules to form solvation shells, resulting in solvated carriers with a larger Stokes radius[15]. During electrochemical reactions, desolvation at the electrode/electrolyte interface emerges as a critical step influencing reaction kinetics, thereby directly impacting the power density of the battery system. In addition to the sluggish kinetics and structural degradation caused by large ion radii, inorganic cathode materials typically contain transition metal elements, which pose a risk of dissolution into the electrolyte during electrochemical reactions, leading to structural collapse and capacity fading. For example, in P2-type Mn-based layered oxides, Mn^{2+} generated during cycling has a high solubility in the electrolyte, leading to loss of reversible capability of the cathode[16]. This issue is

---

[1]Department of Chemical and Biological Engineering, The Hong Kong University of Science and Technology, Hong Kong SAR, China. [2]Energy Institute, The Hong Kong University of Science and Technology, Hong Kong SAR, China. [3]These authors contributed equally: Suleman Suleman, Xiaolong Cheng.
e-mail: yoonseobkim@ust.hk

particularly pronounced in aqueous multivalent metal-ion batteries, where the high polarity of water molecules and pH fluctuations during electrochemical reactions aggravate the dissolution and corrosion of transition metal elements, leading to accelerated degradation[17].

Compared to the rigid crystalline structures of inorganic cathode materials, organic materials exhibit inherent flexibility, enabling them to accommodate the insertion and extraction of large-radius ions without structural degradation[18,19]. Besides, organic cathodes exhibit unique merits owing to their distinct physicochemical properties, such as tunable redox groups, counterion adaptability, low cost, and environmental friendliness[20,21]. The "soft" properties and polar functional groups of organic cathodes enable flexible accommodation for various charge carriers without inducing large internal stress. As a result, organic materials have emerged as exceedingly promising electrode materials and have garnered significant attention for beyond LIBs[22]. The structural diversity of organic materials and molecular engineering offers a wide range of possibilities, ample space for enhancement, and the capacity to systematically adjust their electrochemical properties using various functional groups. These key features enable diverse synthetic routes and versatile functionalization. However, some small organic molecule-based cathodes usually suffer from solubility issues, which lead to capacity fading during long-term cycling processes, which can be addressed by ordered integrating into polymerized rigid frameworks[23]. For the HMIBs under development, the electrolyte has not been determined. Some nucleophilic electrolytes may aggravate the dissolution of organic electrode materials[24,25]. The organic cathode materials, after common polymerization, become nonporous, hindering the transport of charge carriers. The obstructed electric and ionic conductivity of organic cathodes directly affect the rate capability of the batteries and lead to capacity decay during the cycling process due to the loss of electrical contact, which can be addressed via rational structural design of the electrode materials. Besides, battery performance is also affected by the nonporous nature of many organic electrode materials, which leads to inefficient active site utilization, sluggish ion transport, complicated structure-activity relationships, etc[26,27].

Furthermore, the reaction mechanisms of organic cathode materials are still under investigation, especially in the HMIB systems. Compared with alkali metal-ion batteries, HMIBs usually exhibit complex charge storage mechanisms owing to the coexistence of diverse charge carriers. For example, proton co-storage with M^{2+} mechanism has been found in the ZIBs and CIBs; in some battery systems, such as dual-ion batteries, anions, e.g., Cl^-, $CF_3SO_3^-$, SO_4^{2-}, etc., also participate in charge storage. Moreover, metal ions usually form various solvation structures with solvent molecules and anions, which makes the storage mechanism much more complicated. Besides, compared with alkali metal ions (Li^+, Na^+, or K^+), the high charge density of multivalent metal ions raises some unique challenges in HMIBs, which are mainly due to the spatial site resistance and underlying co-intercalation of anions during charge/discharge process[28]. Taking the calix [4] quinone (C4Q) molecule as an example, it can bind 8 Li^+, but can only store 4 or fewer charges in the HMIBs, owing to intensified coulombic interactions between metal ions and anions in the electrolyte[29]. Therefore, in-depth research on the charge storage mechanism based on the designed molecular structure model is of great significance for the development of the HMIBs. To address the challenge associated with organic electrodes, plenty of approaches have been proposed, including augmenting the density of redox-active groups to improve specific capacity, modifying the functional group and spatial arrangement of the active group to optimize the voltage profile, structural modulating and compositing with conductive substance to improve cycling stability. As a result, well-designed molecular structure and nano-microstructure of the organic cathode materials play a vital role in the development of next-generation beyond-LIBs with long lifespans, high power density, and mass-energy density[30,31].

Covalent organic framework (COF)-based cathodes

Gratefully, the diversity of organic materials presents various opportunities to enhance designability. One viable approach is extending molecular materials into two-dimensional (2D) and three-dimensional (3D) organic frameworks[32]. Among these frameworks, COFs stand out due to their abundant ordered pores, high crystallinity, and high surface areas, which have been considered excellent platforms for constructing controllable materials with specific performance characteristics[33–36]. In recent years, COFs have attracted substantial attention from many engineering fields, including gas storage, separation, catalysis, and sensors[37–40]. Notably, their potential in electrochemical energy storage applications has been gaining momentum[41,42]. COFs are considered highly promising electrode materials due to their inherent insolubility in electrolytes, controllable pore size, significant porosity, well-structured open channels for ion transport, and π-conjugated frameworks that facilitate charge transport[43,44]. Their lightweight elemental composition (primarily C, H, O, N) and abundant active sites directly contribute to high gravimetric energy density. Furthermore, the unique crystalline structure of COFs facilitates proximal active sites and functional groups to coordinate with alkali and multivalent ions through chelation or V-type interactions inherent to COF architectures. This facilitates efficient ion migration and storage while stabilizing the charged and discharged states[45,46]. Combined with the abundant and well-defined pore structures of COFs, the transport of multivalent ions with large radii is significantly enhanced. Additionally, the presence of multipolar functional groups facilitates the desolvation of charge carriers, thereby improving the reaction kinetics of the cathode. Besides, rational structure design can enhance the stability of COFs at high voltage conditions. For example, Niu et al. convert the imine linkage to quinolyl linkage to obtain the Q-COF, which exhibits significantly enhanced high-voltage stability (5.6 V)[47]. Similarly, defective COFs with imidazolium[48], sulfonate groups in hydrazone-linked COF nanosheets (4.5 V)[49], imidazolium groups in cationic imine-linked COFs (4.2 V)[50], and cationic moieties in cationic hydrazone-linked COF nanosheets (3.8 V)[51] display significantly improved high-voltage stability. Here, we showcase the timeline and important progress of COF-based cathodes in the development of batteries in the last five years (2019-2024), which extend beyond traditional LIB technology (Fig. 1a). In recent years, significant advancements in COF-based cathode batteries have garnered considerable global interest due to several noteworthy characteristics, including the high natural abundance of the materials, their low reactivity under atmospheric conditions, and their capacity for facilitating high-electron redox reactions. The data presented indicates a significant exponential increase in the publication output concerning COF-based cathodes beyond the LIB systems (Fig. 1b). Based on a comprehensive review of published reports on cathode materials for beyond-LIBs, we have systematically evaluated the electrochemical performance, cost, and safety metrics of various cathode material types, including inorganic cathodes, organic cathodes, and COF-based cathodes, which are presented in radar charts form (Fig. 1c–e). Generally, COF-based cathode materials exhibit significant advantages in gravimetric energy density and specific capacity due to their lightweight elemental composition and abundant active sites. However, their volumetric energy density lags behind traditional inorganic cathode materials owing to their porous structures and low density. Furthermore, the exclusion of transition metal elements in COF-based cathode materials positions them as cost-effective alternatives, with the potential for significant cost reduction upon industrialization. In terms of safety, COF-based cathodes demonstrate exceptional thermal and chemical stability, maintaining structural integrity during cycling, which ensures robust safety performance. Leveraging these characteristics, COF-based beyond-LIBs hold significant promises for industrialization and deployment in applications where volumetric energy density is less critical, but gravimetric energy density, cycle life, safety, and low cost are prioritized, such as future grid-scale energy storage systems.

Approaches to advance COF-based cathodes

The structural versatility of COFs provides an excellent opportunity to enhance their electrochemical performance via thoughtful and controlled molecular-level design. The primary elements of COFs—such as redox sites, building units, and functional groups—along with their molecular framework and conjugated structure, can be adjusted to significantly affect

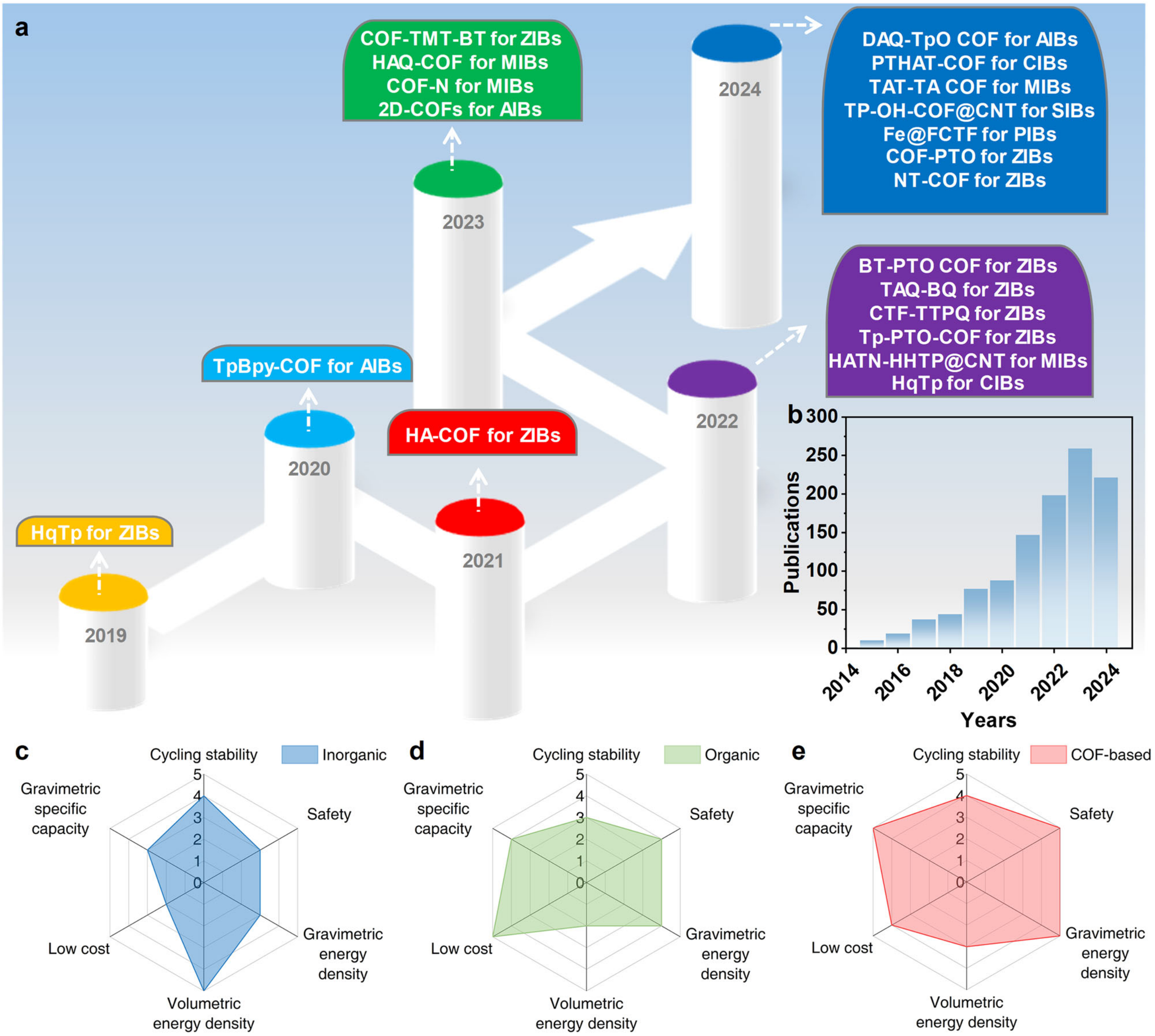

Fig. 1 | Overview and trends of COF-based cathodes beyond LIB applications. **a** Chronological overview of developments for the period 2019–2024. Reference examples include hydroquinone linked β-ketoenamine COF (HqTp)[115], 2,2′-bipyridine moieties based COF (TpBpy-COF)[100], 1,4,5,8,9,12-hexaazatriphenylene-based COF (HA-COF)[53], orthoquinone-based COF (BT-PTO COF)[63], anti-aromatic COF (TAQ-BQ)[134], quinoxalinophenazinedione CTF (CTF-TTPQ)[135], carbonyl-rich COF (Tp-PTO-COF)[74], hexaazatrinaphthalene-based COF (HATN-HHTP@ carbon nanotube (CNT)[136], hydroquinone linked β-ketoenamine COF (HqTp)[98], olefin-linked COF (COF-TMT-BT)[91], quinone functionalized 1,4,5,8,9,12-hexaazatriphenylene-based COF (HAQ-COF)[137], polyimides-based COF (COF-N)[127], polyimide 2D COF (2D-PT-COF)[96], carbonyl-rich DAQ-TpO COF[101], pyrazine-pyridinamine COF (PTHAT-COF)[57], azatruxene COF (TAT-TA COF)[97], TP-OH-COF@CNT50[79], carbonyl-rich COF with pyrene-4,5,9,10-tetraone groups (COF-PTO)[118], donor-acceptor configuration COF (NT-COF)[119]. **b** Publication trends numbers on the topic of “Covalent organic frameworks” and “Batteries” from 2014–2024. The data was generated from the Web of Science. **c**–**e** The radar plots of inorganic cathodes, organic cathodes, and COF-based cathodes.

electrochemical performance[52–54]. For critical performance indicators in rechargeable batteries, such as theoretical specific capacity, redox potential, and rate performance, various principles of molecular-level design have been introduced to develop suitable COFs as electrode materials, establishing connections between structure and performance[55,56].

Design and preparation of COF-based cathodes

The versatility of COFs is evident in the diverse range of lattice structures that can be achieved by combining monomers with different symmetries, including representative hexagonal, tetragonal, rhombic, Kagome, and trigonal topologies[57–60]. The design of these COFs often involves using monomers with rigid π backbones, which enable the formation of directional connections between knots and linkers. These monomers typically possess distinct geometries that delineate the relative positions of their reactive sites. The directions for polymer chain development can be meticulously aligned with a predefined topology, as covalent bonding governs spatial orientation and establishes the relative positioning of interconnected monomer units. For example, the connection of planar monomers constraints on the growth of polymer backbones, facilitating the formation of 2D atomic layers with engineered topologies. Furthermore, organic monomers with rigid backbones frequently incorporate π-systems. When these π-units within the 2D covalent polymers are judiciously oriented, the resulting rigid 2D polymers preferentially adopt layered structures, wherein interlayer interactions predominantly dictate the overlap between adjacent layers. This strategic alignment culminates in forming highly aligned 2D COFs in AA stacking, oriented along the z-axis. Furthermore, the design of monomers is essential for incorporating functionalities into COFs, which can markedly enhance their performance in batteries. Numerous studies have demonstrated that

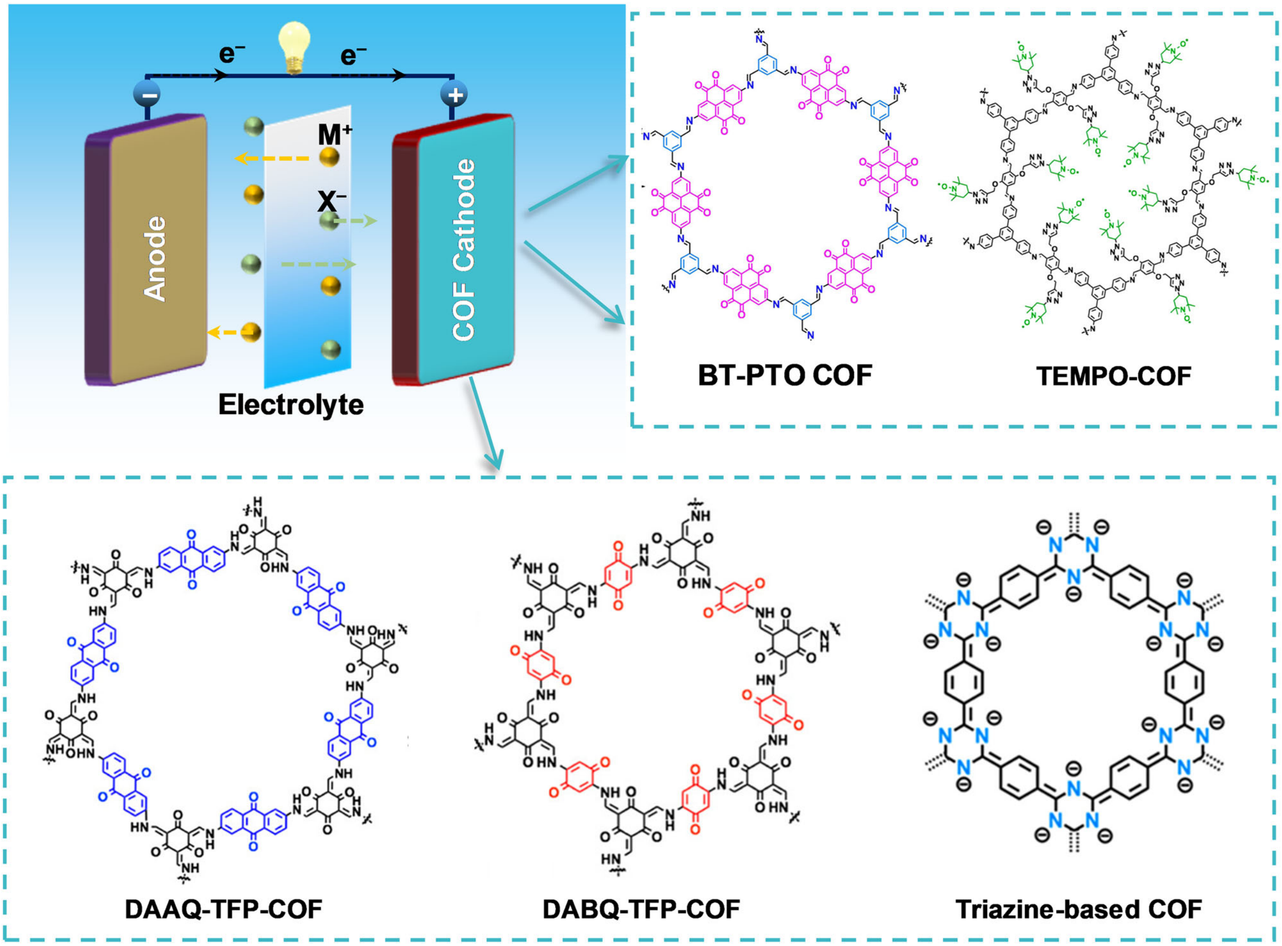

Fig. 2 | Schematic figure of the working principles of COFs for beyond LIBs. The representative COFs, BT-PTO COF[63], TEMPO-COF[64], DAAQ-TFP-COF[64], DABQ-TFP-COF[64], and Triazine-based COF[65], showcase the various redox centers in COF-based cathodes.

monomers featuring redox-active carbonyls, hydroxyl groups, ethers, conjugated nitrogen, or conjugated C–C bonds effectively bind with K^+, Zn^{2+}, Ca^{2+}, Al^{3+}, and Mg^{2+}. An alternative strategy for introducing functional groups involves post-synthetic modification[61,62].

The charging and discharging processes of COF-based cathodes in beyond-LIBs primarily rely on the rocking-chair motion of anions and cations coupled with reversible electrochemical reactions at the electroactive organic groups, where charge states are reversibly altered. (Fig. 2)[63–66]. These COFs, which include carbonyl-rich structures, 2,2,6,6-tetramethylpiperidine 1-oxyl radicals (TEMPO), triazine rings, etc., serve as redox centers for storing various metal ions in the cathodes. The unique combination allows for efficient energy storage and release, enhancing the overall performance of the batteries.

Generally, the electrochemical reaction in the battery consists of three key parts: the conduction of electrons, the transport of ions, and the charge transfer process. The intrinsic electrical conductivity of most COFs is low, which is the "short slab" and raises the challenge of optimization. Increasing conductivity by enhancing the conjugated structure and introducing conductive agents usually leads to reduction in active redox-site density and decrease in specific capacity. Appropriate porosity assists to accelerate the transport of ions and reduce polarization. Pores that are too large will lead to a bloated structure and increase the distance for electron transmission. Thus, balancing conductivity, redox activity and the nano-microstructure (porosity and specific surface area) plays an important role in the development of COF-based cathodes.

This review delineates the developmental trajectory of COF-based cathodes for applications beyond LIBs, emphasizing their potential in HMIBs, as well as SIBs and PIBs. We summarize recent advancements in designing COFs and analyze the relationship between their chemical designs and electrochemical performance. Additionally, we discuss strategies for constructing COFs to enhance their electrochemical properties, identify key challenges, and propose future research directions to guide the development of COFs for energy storage applications.

Methodology for electrochemical performance optimization

Molecular structure regulation

Redox-active group manipulation. The electrochemical behavior of the COFs is influenced by redox-active functional groups, which can be classified as n-type, p-type, or bipolar[27,67–69], where n-type groups[63,70] accept electrons to interact with metal ions via reduction-oxidation, while p-type functionalities[71,72] facilitate pseudocapacitive anion (ClO_4^-, PF_6^-, BF_4^-, and $TFSI^-$) interactions through reversible neutral/positively charged transitions. A bipolar system, unify n- and p-type moieties within a single framework, enhancing energy/power density by enabling dual redox states[73]. Particularly, increasing redox-active groups while minimizing inactive ones is critical to effectively enhancing theoretical specific capacity. In this context, Tao et al. designed a BT-PTO COF, using benzenetricarboxaldehyde (BT) as the node and 2,7-diaminopyrene-4,5,9,10-tetrone (PTO) as building blocks. The carbonyl-rich active site of the PTO component enabled the COF to achieve a remarkable reversible capacity of 225 mAh g^{-1} at a current density of 1 A g^{-1} (Fig. 3a, b)[63]. Furthermore, the proposed H^+ and Zn^{2+} co-insertion mechanism in the BT-PTO COF cathode shows that during discharge, Zn^{2+} ions insert first, followed by two H^+ ions, driven by redox pseudocapacitance. Subsequently, this process reverses during charging,

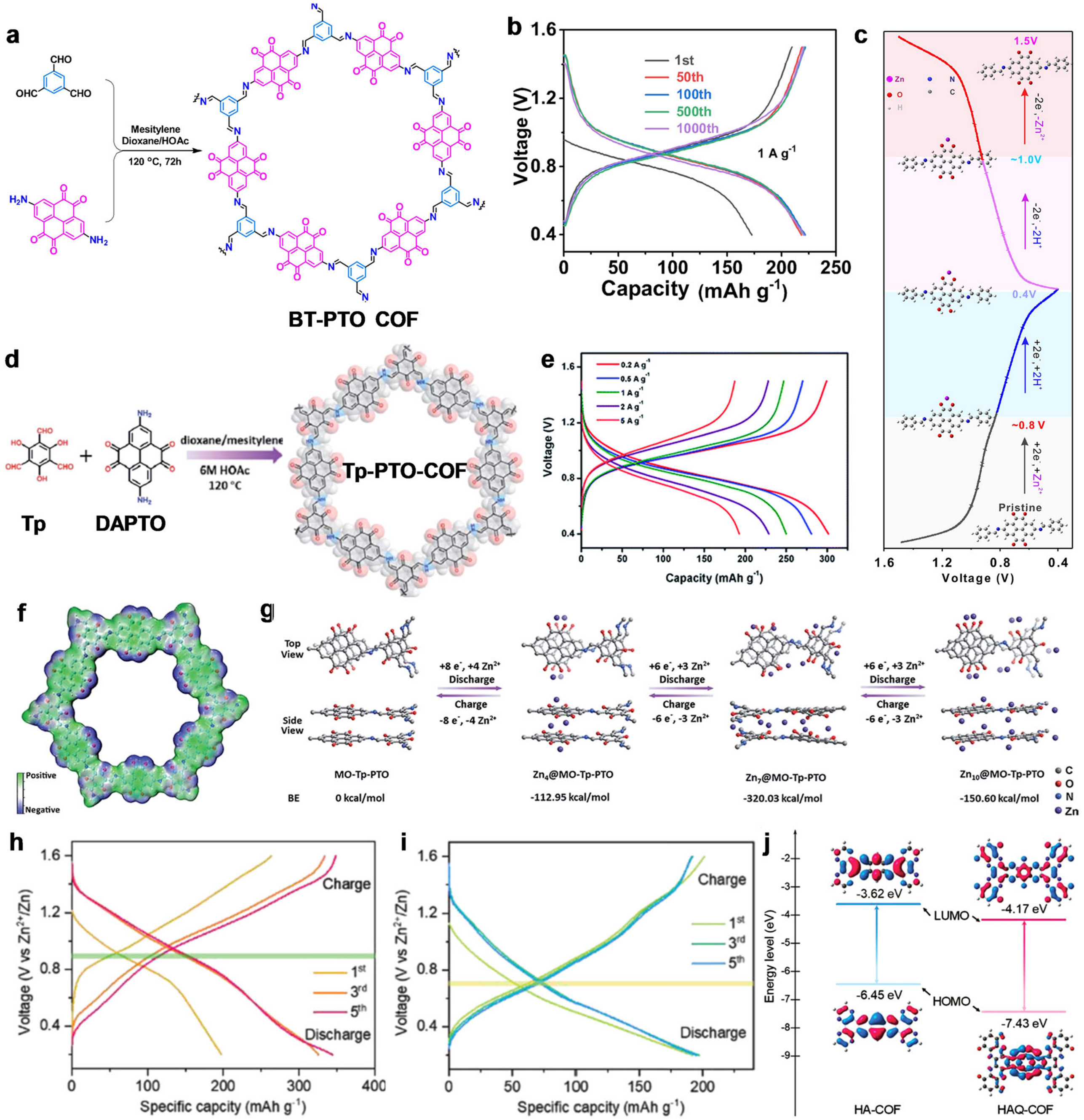

Fig. 3 | Redox-active group installed in COFs to facilitate ion coordination and conduction. **a** Schematic representation of the BT-PTO COF. **b** Charge–discharge profiles of BT-PTO COF at various current densities. **c.** BT-PTO COF proposed H^+, and Zn^{2+} co-insertion routes. Reproduced with permission[63]. Copyright 2022, Wiley-VCH. **d** Illustration of the synthetic route to Tp-PTO-COF. **e** Galvanostatic charge–discharge curves of Tp-PTO-COF at different current densities. **f** MESP of Tp-PTO-COF. **g** BE simulations with varying quantities of Zn^{2+} ions in MO-Tp-PTO. Reproduced with permission[74]. Copyright 2022, Royal Society of Chemistry. **h** Capacity versus voltage data for HAQ-COF. **i.** HA-COF in a 2.0 M $ZnSO_4$ aqueous electrolyte, within a potential range of 0.2 to 1.6 V. **j** DFT-derived electronic structures showing the highest occupied molecular orbital (HOMO)-LUMO orbitals and energy levels of HA-COF and HAQ-COF units. Reproduced with permission[53]. Copyright 2021, Wiley-VCH.

with H^+ deinsertion occurring first, followed by Zn^{2+} extraction, highlighting the COF's ability to stabilize multiple ion insertions and contributing to its better performance and cycling stability (Fig. 3c). Moreover, Liu et al. synthesized Tp-PTO-COF using 1,3,5-triformylphloroglucinol (Tp) and PTO as building blocks. The COF featured double active sites, consisting of *β*-keto carbonyl and adjacent carbonyl groups, which facilitated the storage of Zn^{2+}. As a result, Tp-PTO-COF achieved a reversible capacity of 301 mAh g^{-1} at 0.2 A g^{-1} and maintained a high capacity of 193 mAh g^{-1} even at a high current density of 5 A g^{-1} (Fig. 3d, e)[74]. Furthermore, the molecular electrostatic potential (MESP) of Tp-PTO-COF revealing negative regions near the carbonyl groups, indicating strong chemical affinity for cation uptake, particularly for Zn^{2+} ions (Fig. 3f). Notably, the carbonyl group of PTO exhibits the lowest MESP value (−19.66 kcal mol^{-1}), identifying it as the primary site for Zn^{2+} storage. Additionally, the binding energy (BE) simulations of Tp-PTO-COF with varying numbers of Zn^{2+} ions demonstrate that the Zn_{10}@MO-Tp-PTO configuration possesses the most negative BE (−320.03 kcal mol^{-1}), signifying high stability (Fig. 3g). These findings collectively support the proposed mechanism, where Zn^{2+} ions coordinate with carbonyl groups during discharge and uncoordinate during charging, enabling efficient and reversible energy storage. Notably, from the

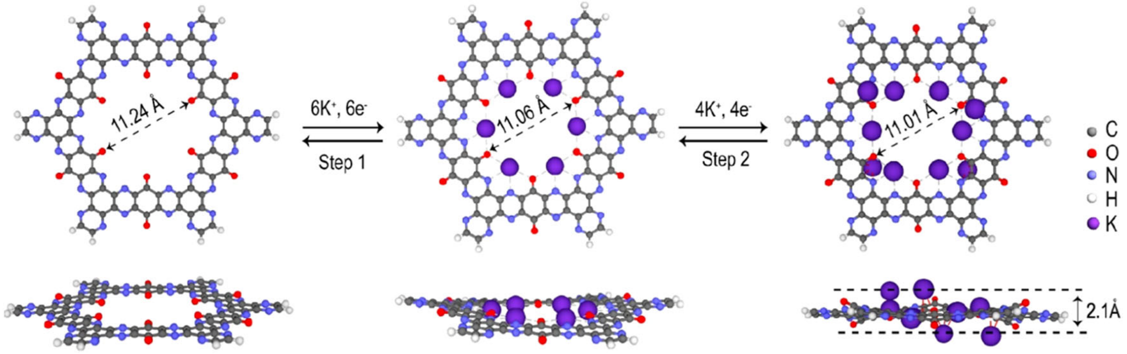

Fig. 4 | Schematic representation of the top and side views of the two-step K$^+$ intercalation and deintercalation process for the TQBQ-COF electrode. Reproduced with permission[76]. Copyright 2023, American Chemical Society.

given discussion, we can learn that the number of redox centers is highly correlated with the battery performance.

The energy density of batteries is influenced by both discharge-specific capacity and average output voltage. Improving specific capacity and increasing the redox potential of cathodes are key research areas for achieving higher energy density. For example, Wang et al. demonstrated that incorporating quinone groups (C=O) groups as electron-withdrawing units into the framework of the HAQ-COF significantly enhances its electrochemical performance, resulting in a higher discharge voltage (0.84 V) compared to the HA-COF (0.53 V) in aqueous ZIBs[53]. The improved performance is attributed to the introduction of quinone groups, which lower the lowest unoccupied molecular orbital (LUMO) energy level of HAQ-COF, thereby elevating its redox potential. Density functional theory (DFT) computations were utilized to investigate the electronic structures and relative energy levels of HAQ-COF and HA-COF (Fig. 3h–i). The results indicate that incorporating quinone groups in HAQ-COF facilitates extended electron delocalization along its backbone, enhancing redox activity. The calculated LUMO energy levels for HAQ-COF (−4.17 eV) and HA-COF (−3.62 eV) demonstrate that the introduction of quinone groups lowers the LUMO energy level, thereby increasing electron affinity and reduction potential, which aligns with experimental observations (Fig. 3j).

Conjugation structure construction. Except for the active redox sites, conjugation engineering also plays an important role in regulating the performance of the COF-based cathode. The conjugated systems can effectively stabilize the molecular structure during cycling processes and facilitate charge transfer owing to the delocalized electron system and reduced energy gap. For example, Yang et al. prepared the BQQPH with six –C=N and six –C=O active groups, which boosted an expanded π-conjugated system, thus yielding an elevated voltage of 1.45 V and enhanced rate capability in AIBs system[75]. Expanding π-conjugated systems can boost the electric conductivity and charge transfer processes, leading to enhanced electrochemical performance. Therefore, the efficient use of active functional groups and a backbone chain of alternating double and single bonds to build conjugated systems can balance the capacity and reaction kinetics of COF-based cathode. During the intercalation and deintercalation of metal ions, the structural properties of COFs, such as pore sizes and electron delocalization, change accordingly. Taking the TQBQ-COF as an example, the pore size slightly shrinks during the insertion of K$^+$ and the conjugation structure react with K$^+$ via the cation-π effect (Fig. 4)[76]. Therefore, constructing COF cathodes with suitable pore sizes, rigid monomers and stable conjugated structure is beneficial for rapid ion and electron transport, as well as fast reaction kinetics and structural stability during the charge and discharge process.

Micro/nano-structural design

Unveiling 2D morphology through exfoliation techniques. Porous channels in redox-active COFs significantly enhance the transport of electrolyte ions compared to nonporous organic materials. However, bulk COF samples often fail to fully leverage these advantages due to their tightly packed layers, which restrict ion penetration[77]. Therefore, an efficient exfoliation strategy is helpful for improving ion diffusion and exposing a greater number of active sites[78]. In this regard, Wang and his team developed a robust method for exfoliating COFs into thin 2D nanosheets via a ball-milling approach (Fig. 5a)[64]. This technique effectively disrupts π-π stacking interactions while preserving the chemical integrity of the COF layers. By fine-tuning the vibration frequency and milling duration, the authors controlled the nanosheet thickness. The resulting few-layer 2,6-diaminoanthraquinone-triformylphloroglucinol COF, DAAQ-ECOF, showed remarkable rechargeability with 98% capacity retention after 1800 cycles, alongside impressive charge-discharge capabilities, retaining 74% at 500 mA g^{-1} compared to 20 mA g^{-1}. Additionally, DABQ-ECOF achieves a specific capacity of 210 mA h g^{-1} with a consistent voltage plateau of 2.8 V, highlighting that the improved kinetics and increased Li$^+$ diffusion coefficients in DABQ-ECOF facilitate greater utilization of active sites, resulting in a predominantly surface-driven pseudocapacitive behavior (Fig. 5b–e). The DABQ ECOF is widely recognized as a pioneering study on COF-based cathodes for LIBs. However, since the primary focus of this work lies beyond-LIB systems, the inclusion of LIB-based COFs warrants further clarification. This is particularly relevant because insights gained from LIB-based COFs, such as ion transport mechanisms, redox-active site engineering, and structural stability, provide foundational principles that can be extended to other metal-ion batteries (e.g., Na$^+$, K$^+$, Zn^{2+}, Mg^{2+}, etc). By leveraging these principles, researchers can accelerate the development of COF-based cathodes for emerging battery technologies, ensuring a more comprehensive understanding of their potential across diverse energy storage systems.

Amplifying performance with micro-nanostructure design. Despite substantial research efforts to enhance COF-based cathode materials through molecular engineering, their performance still falls short of practical requirements. Adopting material-level approaches, such as integrating conductive components or optimizing microstructure, are widespread strategies for further improving COF performance. Yuan et al. reported a TP-OH-COF, which was synthesized through one-step in-situ polycondensation and combined with CNT, resulting in a few-layered structure rich in redox-active groups (Fig. 6a)[79]. This design enhances Na$^+$ accommodation and reduces ion/electron diffusion distance when the TP-OH-COF wraps around the CNTs. As a cathode for SIBs, TP-OH-COF@CNT50 achieves a specific capacity of 256.4 mAh g^{-1} at 0.1 A g^{-1}, demonstrating excellent cycling stability and rate performance. Furthermore, the MESP of TP-OH-COF highlighting the minimum electrostatic potential values around the carbonyl groups, which indicates their high reactivity and suitability as primary sites for Na$^+$ ion storage. Moreover, the optimized structure of TP-OH-COF binding with Na atoms, revealing that Na$^+$ ions preferentially bind to the carbonyl groups of the Pa-OH, unit with a Na-O bond distance of 2.14 Å, while the TP unit stabilizes Na$^+$ ions with a slightly longer bond distance of 2.19 Å (Fig. 6b). Further insight was obtained from

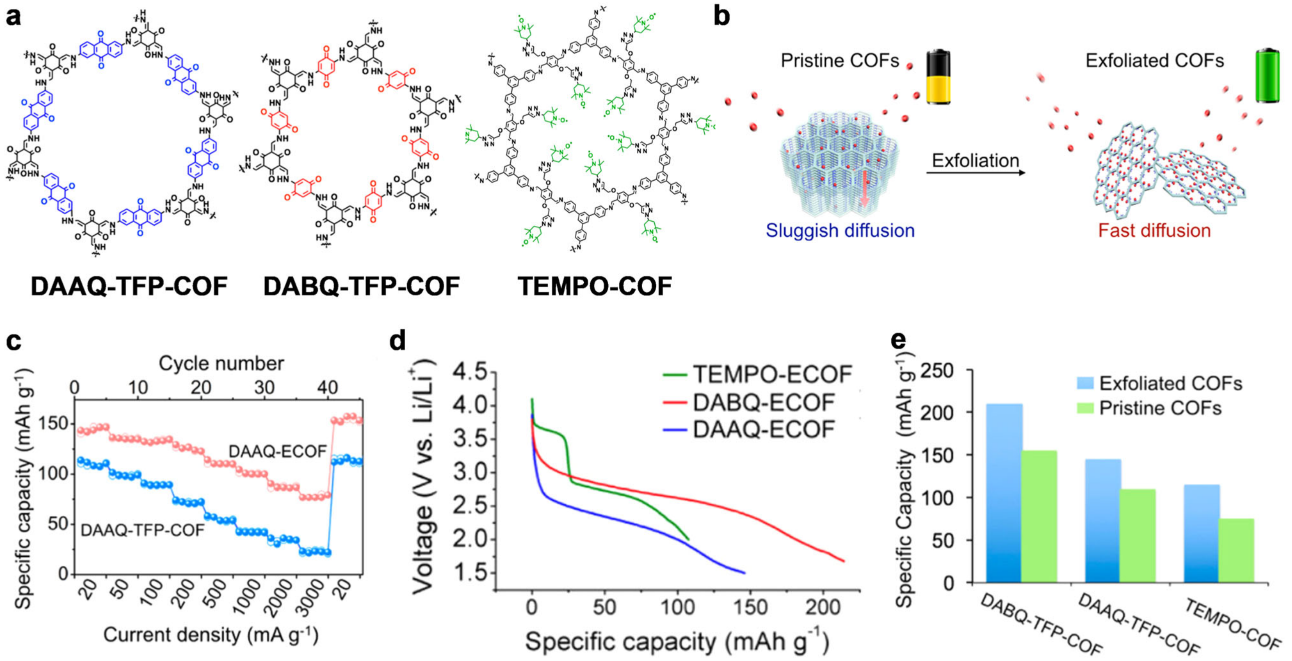

Fig. 5 | Exfoliated redox-COFs showing improved capacity over bulk counterparts. **a** Structures of COFs, DAAQ-TFP-COF, DABQ-TFP-COF, and TEMPO-COF. **b** Exfoliation diagram for 2D COFs. **c** Performance rates measured during testing. **d** Discharge profiles at a current rate of 20 mA g^{-1}. **e** comparation of capacity between pristine and exfoliated COFs at 20 mA g^{-1}. Reproduced with permission[64]. Copyright 2017, American Chemical Society.

the total energy and free energy (ΔG) profiles for the stepwise sodiation process, which demonstrated that the binding of Na^+ ions to TP-OH-COF is exergonic. The energy decreases as more Na^+ ions are incorporated, indicating stable adsorption. These results collectively confirm that the carbonyl groups in TP-OH-COF are the key active sites for reversible Na^+ ion storage, contributing to the materials high electrochemical performance. In a related approach, Duan et al. developed a few-layered COFs integrated with carboxylated CNTs for PIBs (Fig. 6c)[80]. The ESP calculation of the repetitive structure unit of DAAQ-COF reveals that the $C=O$ groups are highly reactive sites for K^+ adsorption (Fig. 6d). Further, the optimized structures of the DAAQ unit binding with one and two K^+ ions, indicating that K^+ preferentially binds with the $C=O$ groups, with bond distances of 2.59 Å and 2.84 Å, respectively (Fig. 6e). Moreover, the total energy and free energy profiles for the step-by-step potassiation process, demonstrating that the binding of to the DAAQ structure is exergonic, with two K^+ binding being more favorable (Fig. 6f). These results suggest that the DAAQ-COF structure can stably accommodate two K^+ ions, aligning with the experimental capacity findings.

Application of COF-based cathodes for beyond LIBs

Critical analysis of alternative battery technologies

As alternatives to LIBs, batteries utilizing Na^+, K^+, Mg^{2+}, Ca^{2+}, Al^{3+}, and Zn^{2+} as charge carriers are valued for their abundant element resources in the Earth's crust, appropriate redox potentials, and other physicochemical properties (Table 1). However, the large ionic radius of these charge carriers leads to sluggish reaction kinetics, creating stringent requirements for the selection and design of positive electrodes, particularly in multi-electron reaction systems.

Similar to LIBs, the development of alternative battery technologies are closely correlated with the extensive investigation of various cathode materials, which directly determine the capacity and energy density of battery devices. Traditional inorganic cathodes for MIBs, such as transition metal oxide, polyanion, and Prussian blue analogs, often face challenges such as volumetric variation, dissolution of transition metal ions, and phase transitions, resulting in performance degradation. As counterparts to inorganic cathodes, organic cathodes composed of light nonmetal elements show many typical merits, such as designable and abundant molecule structure, low atomic weights, and thus high theoretical gravimetric capacities, and flexible molecular structure for reversible accommodation of large charge carriers. However, many kinds of organic electrode materials usually suffer from dissolution in organic electrolytes, leading to the degradation of batteries. In this context, COF-based materials, with adjustable molecular structures, abundant active sites, stable crystal frameworks, and unique porous structures, are considered promising candidates for effective cathode materials. Various functional groups, including carbonyl, ether, and imine, can reversibly store metal ions during the charge/discharge process by breaking and forming chemical bonds and electrostatic adsorption. The nanoscale pores allow metal ions and various anions to move quickly in a "rocking chair" style while keeping the crystal structure intact.

SIBs and PIBs

SIBs are emerging as promising energy storage solutions for large-scale applications due to their abundance and cost-effectiveness compared to Li-based systems[81]. However, the relatively greater ionic radius of Na^+ (1.02 Å) compared to Li^+ (0.76 Å) leads to reduced ion transport efficiency and increased volume changes during the reversible cycling process[82]. This poses a considerable challenge in attaining high-rate capability and cycle performance. In this context, numerous COFs have been identified as promising electrode materials for SIBs, leveraging their adjustable pore sizes and versatile chemical structures to mitigate significant volume expansion and enhance ion transport efficiency[71,83,84]. Recently, Yuan et al. reported the TP-OH-COF, having abundant redox-active groups (C=O), with CNTs (denoted as TP-OH COF@CNT50) through a one-step in situ polycondensation process for cathode materials in SIBs (Fig. 7a)[79]. This few-layered TP-OH-COF, accommodating maximum number of Na^+ while effectively reducing the diffusion distances for both ions and electrons, exhibited a remarkable specific capacity of 256.4 mAh g^{-1} at a current density of 0.1 A g^{-1}, along with exceptional cycling stability, demonstrating 100% retention after 3000 cycles at 2 A g^{-1}, and impressive rate performance, achieving 103 mAh g^{-1} at 10 A g^{-1} (Fig. 7b). The combination of in situ and ex situ experiments revealed a highly reversible surface-

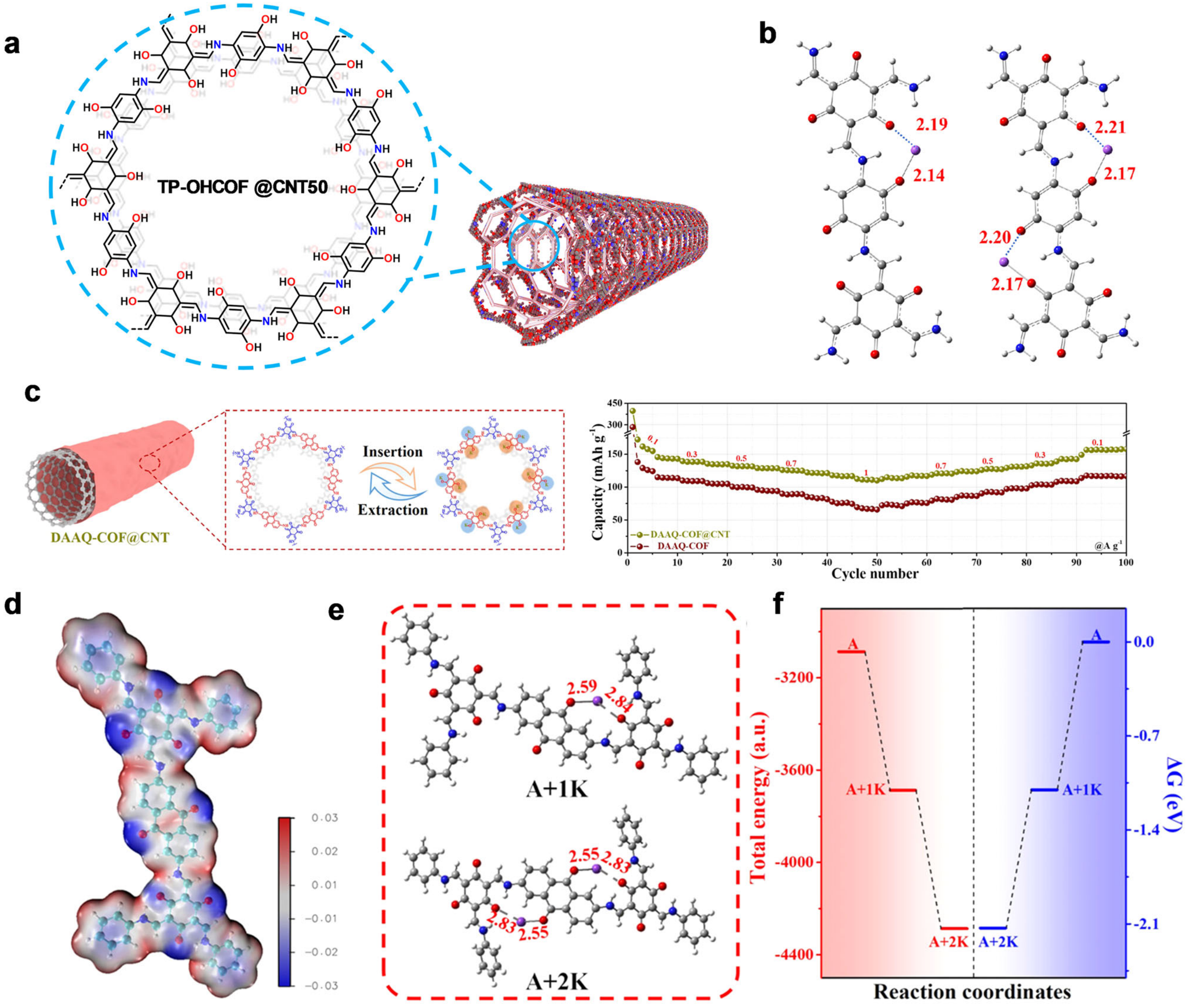

Fig. 6 | COFs grown on CNTs to improve the cathodes' performance. **a** Scheme of TP-OH-COF on CNTs. **b** Structural model of Na$^+$ interaction with TP-OH-COF. Reproduced with permission[79]. Copyright 2024, Elsevier. **c** Schematic depiction of DAAQ-COF@CNT. **d** ESP visualization of DAAQ-COF. **e** Structural models of K$^+$ interaction with DAAQ-COF. **f** Thermodynamic analysis of K$^+$ interaction with DAAQ-COF. Reproduced with permission[80]. Copyright 2022 American Chemical Society.

Table 1 | General properties comparation of different metal elements[107,108]

Elements	Atomic No.	Redox potential (V vs. SHE)	Ion radius (Å)	Hydrated ion radius (Å)	Earth crust abundance (%)	Gravimetric capacities (mAh g^{-1})
Li	3	−3.04	0.76	3.40	0.0018	3860
Na	11	−2.71	1.02	2.76	4.15	1166
K	19	−2.93	1.38	2.01	2.09	685
Mg	12	−2.37	0.72	3.00	2.33	2206
Al	13	−1.66	0.54	4.8	8.23	2980
Ca	20	−2.87	1.0	4.12	4.15	1337
Zn	30	−0.76	0.74	4.04	0.0079	820

dominated mechanism for Na$^+$-storage and confirmed the structural stability of TP-OH-COF@CNT50, which features a lower energy barrier for Na$^+$ diffusion during insertion and extraction processes (Fig. 7c). Furthermore, Shi et al. developed a nitrogen-rich COF (TQBQ-COF) with a honeycomb-like structure for SIBs cathodes[85]. In situ Fourier transform infrared spectroscopy and ex situ X-ray photoelectron spectroscopy (XPS), along with DFT computations, revealed that both pyrazines and carbonyl groups facilitated Na$^+$ storage. TQBQ-COF accommodated up to 12 Na$^+$ ions per unit, achieving a capacity of 452.0 mAh g^{-1} at 0.02 A g^{-1}. Incorporating nitrogen reduces the band gap, enhancing conductivity and enabling rapid ion transport, resulting in a rate performance of 134.3 mAh g^{-1} at 10.0 A g^{-1}.

PIBs have emerged as a noteworthy type of alkali metal-ion batteries. Their electrochemical potential of K/K$^+$ (−2.94 V vs. SHE) is comparable to Li/Li$^+$ (−3.04 V vs. SHE), providing high voltage and energy density[86]. K$^+$ exhibits superior ionic conductivity and faster diffusion kinetics due to its

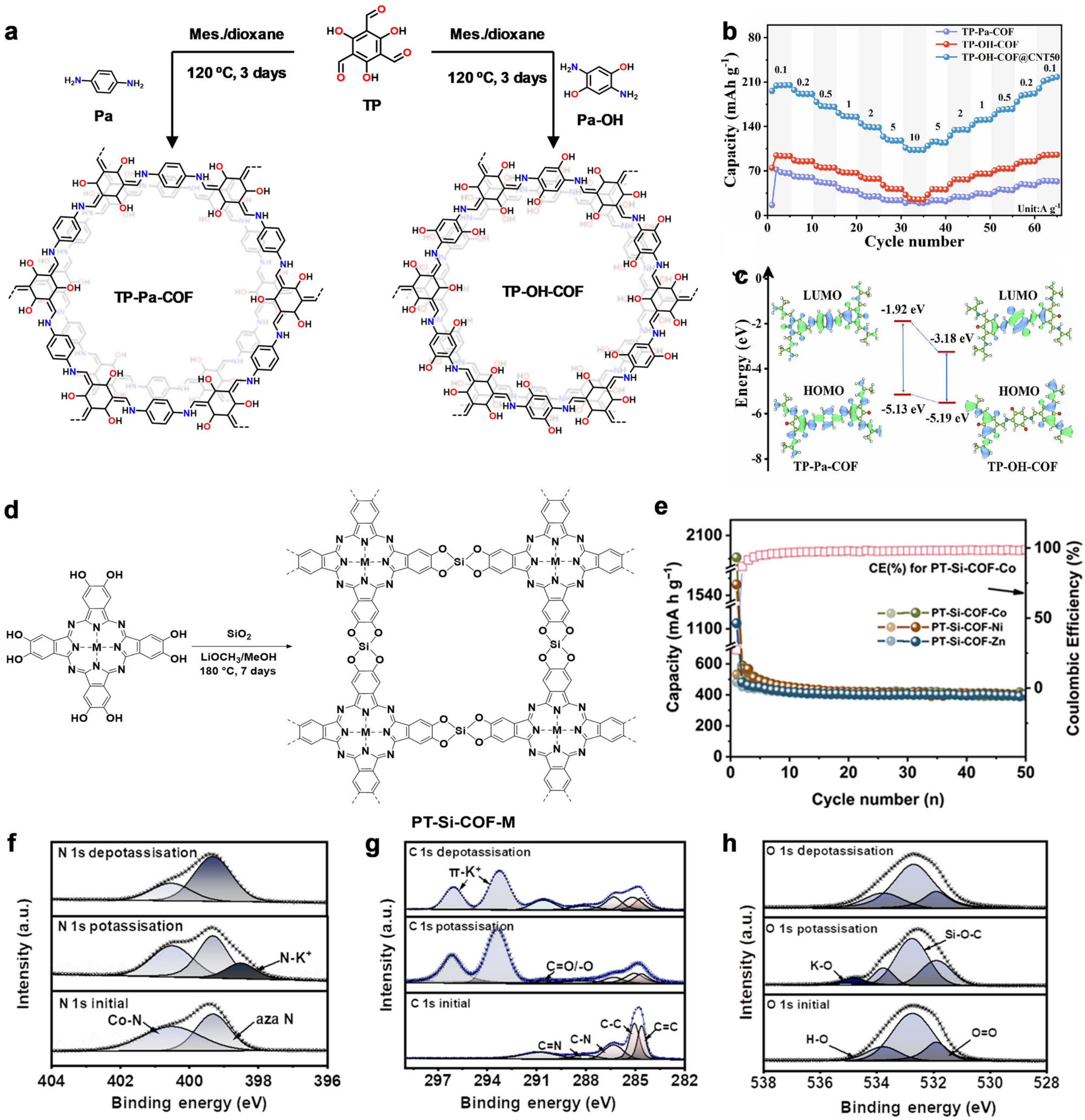

Fig. 7 | COF-based cathodes for SIBs and PIBs. a–d, TP-OH-COF for the cathode in SIBs. **a** Synthesis scheme for TP-Pa-COF and TP-OH-COF. **b** Rate performance comparation of TP-Pa-COF, TP-OH-COF, and TP-OH-COF@CNT50. **c** HOMO/LUMO energy diagrams, along with the corresponding configurations of TP-Pa-COF and TP-OH-COF. Reproduced with permission[79]. Copyright 2024, Elsevier. PT-Si-COF-M for the cathode in PIBs. **d** Schematic representation of PT-Si-COFs synthesis. **e** Cycling performance of the PT-Si-COFs. **f** N 1 s XPS spectra. **g** C 1 s XPS spectra. **h** O 1 s XPS spectra. Reproduced with permission[66]. Copyright 2024, Chinese Chemical Society.

weaker Lewis acidity and lower desolvation energy relative to Li^+. However, the larger ionic radius of K^+ (1.38 Å) limits the availability of compatible electrode materials. This results in electrode degradation and rapid capacity decay due to significant volume expansion. Consequently, there is a critical need for structurally stable cathode materials in high-performance PIBs. In this regard, COFs offer distinct advantages with their robust and porous crystalline structures. Liu et al. recently reported a series of 2D COFs, named PT-Si-COF-M (M = Co, Ni, Zn), which exhibited exceptional anodic K^+ storage performance in PIB (Fig. 7d)[66]. These materials demonstrated a capacity of 384 to 386 mA h g^{-1} at 40 mA g^{-1}, with the PT-Si-COF-Co electrode achieving 386 mA h g^{-1} after 50 cycles and capacity retention of 95% (Fig. 7e). Additionally, the PT-Si-COF-Co electrode showed potassiation and depotassiation capacities of 1958 and 534.7 mA h g^{-1}, respectively, although it has an initial coulombic efficiency of only 27.3% due to the formation of solid electrolyte interface film. Furthermore, it maintained a reversible capacity of 118 mA h g^{-1} after 5000 cycles at 1000 mA g^{-1}, yielding a capacity retention of 78.6%. Furthermore, mechanistic analysis of PT-Si-COFs revealed reversible nitrogen-potassium interactions in the N 1s XPS spectra, characterized by the emergence of a distinct peak at 398.51 eV during potassiation, which subsequently diminished upon depotassiation (Fig. 7f). The C 1s spectra demonstrate reversible changes in carbon bonding states, confirming K^+ involvement with the conjugated phthalocyanine framework (Fig. 7g). The O 1 s spectra exhibit a potassium-oxygen peak at 534.8 eV post-potassiation, indicating SiO_4

linker participation in K^+ storage, which reversibly weakens after deintercalation (Fig. 7h). These findings highlight the potential of these COFs for advanced energy storage applications. In order to directly compare the performance of different cathode materials, the electrochemical performance of various cathode materials for the SIBs and PIBs are summarized in Table 2. Even though the voltage is relatively lower, most COF-based cathodes have significantly better cycling stability than that of inorganic cathodes.

ZIBs

Rechargeable ZIBs have garnered considerable attention recently due to their economical nature and the beneficial low redox potential of Zn^{2+}[55,87]. Even though the Zn metal offers relatively low specific capacity (820 mAh g^{-1}) in comparation with other High-valent metals, such as Ca, Mg, and Al, the configuration with aqueous electrolyte and simple manufacturing make it promising for large-scale energy storage. However, ZIBs face significant challenges related to both positive and negative electrodes. Problems such as electrode dissolution, adverse electrostatic interactions, zinc dendrite formation, corrosion, passivation, and byproduct accumulation can lead to capacity loss, reduced Coulombic efficiency, and potential short circuits. These issues significantly hinder the progress and commercial potential of aqueous ZIBs[88,89]. The characteristic features of COF are stable covalent frameworks, defined porous architectures, and multiple redox-active functional groups. These attributes mitigate positive electrode dissolution and dendrite growth on the negative electrode. Additionally, COF effectively stores Zn^{2+}, making it a promising candidate for rechargeable ZIB electrodes[53]. To obtain a high specific capacity, Yu et al. incorporated a 2D polyimide-COF, which was synthesized from naphthalene diimide and triphenylamine units with CNTs. The layered morphology of the intertwined PI-COF/CNT network promoted multiple pathways for electron transport (Fig. 8a)[90]. DFT simulations indicated that the redox-active carbonyl groups were significantly exposed within the 1D nanochannels of the PI-COF structures (Fig. 8b). Recently, Peng et al. investigated COF-TMT-BT, which incorporates active benzothiadiazole units (Fig. 8c)[91]. This design is predicated on the strategic introduction of highly electronegative atoms, specifically nitrogen and sulfur, into the carbon framework. The performance of the COF-TMT-BT electrode demonstrates impressive capacities of 283.5, 262.2, 232.6, 191.4, and 142.2 mAh g^{-1} at the current densities of 0.1, 0.2, 0.5, 1.0, and 2.0 A g^{-1}, respectively (Fig. 8d). Notably, this study marked the first observation of a stable voltage plateau at 1.2 V on the organic electrode under low current densities, a significant finding for enhancing the average voltage. Furthermore, electronic structure simulations indicated that COF-TMT-BT has a bandgap of 1.11 V, suggesting its excellent theoretical electronic conductivity (Fig. 8e). The electrochemical performance comparation of cathode materials for ZIBs is summarized in Table 3. The specific capacities of COF-based cathodes are higher than those of inorganic cathodes, and some rational structural designs of COFs deliver extremely long lifespan, demonstrating the advantage of COF-based cathodes.

CIBs, AIBs, and MIBs

In pursuing advanced energy storage solutions, researchers have focused on alternatives to traditional LIBs. Most notably, they exhibit a high theoretically specific capacity, which indicates their potential to store substantial amounts of energy relative to their mass[92–94]. In conjunction with these metals, the advantageous properties of COFs arose as promising directions for post-LIB research, including CIBs, AIBs, and MIBs. Among these alternatives, Ca, Al, and Mg have emerged as promising candidates due to their advantageous properties. These metals are characterized by low density and abundant availability in the earth's crust, making them attractive for sustainable energy applications. These advancements underscore the potential of Ca[57,95], Al[96], and Mg[97] in conjunction with COFs, to enhance the efficiency and sustainability of energy storage technologies.

Li et al. were the first to investigate the performance of HqTp COFs in aqueous CIBs (Fig. 9a), highlighting the highlighting co-insertion of protons and Ca^{2+}, and the in-situ conversion of oxygen-containing group[98]. The electrochemical properties of HqTp are influenced by its unique morphology, which features a nano-strip structure with diameters ranging from 50 to 100 nm. This structure increases the surface area for ion interaction, leading to more active sites for charge storage. Additionally, the nano-strips improve contact with the electrolyte, resulting in quicker kinetics during charging and discharging. To examine the prevalent phenomenon of proton cointercalation in aqueous batteries, the authors conducted CV analysis in electrolytes comprising both water and organic solvents, such as ethylene glycol. The resulting CV curves revealed a single pair of redox peaks in ethylene glycol, while two pairs were detected in the water (Fig. 9b). The discharge-charge curve of the HqTp at 0.1 A g^{-1}, highlighting distinct voltage plateaus that correspond to the reversible insertion and extraction of Ca^{2+} ions. The curve indicates a gradual increase in capacity during the initial cycles, suggesting an activation process where more electrochemically active sites become accessible over time (Fig. 9c). Further mechanistic insights were obtained from FTIR and XPS analyses, which revealed the reversible changes in C=O and C-O groups and confirmed the bulk storage of Ca^{2+} ions in the HqTp. These findings highlight the critical role of carbonyl groups in the electrochemical performance of the material (Fig. 9d).

Next, AIBs present a promising avenue as they are characterized by enhanced safety, reduced cost, and greater energy density, making them particularly well-suited for applications in large-scale power grids and electric vehicles. However, the high charge density of Al^{3+} ions, coupled with the strong interactions between Al^{3+} and the host lattice, similar to those observed with Mg-ions, limits the number of suitable cathode materials capable of facilitating the reversible deintercalation of aluminum ions. Consequently, many of these materials present challenges regarding their capacity and life cycle. The most commonly used electrolyte in AIBs is the ionic liquid $AlCl_3$-[Emim]Cl, enabling energy storage via reversible intercalation and deintercalation of $AlCl_4^-$ or $Al_2Cl_7^-$ anions[99]. Inspired by layered graphite's ability to accommodate $AlCl_4^-$, Lu et al. reported 2,2′-bipyridine-based COFs, specifically TpBpy-COF, as the cathode material. powder X-ray diffraction confirmed 2D layered structure that facilitates $AlCl_4^-$ diffusion. Theoretical calculations indicated that TpBpy-COF functions as a semiconductor with a bandgap of 1.59 eV, promoting electron transport. IR spectroscopy showed that C=C bonds remained stable, while C=N bonds changed, indicating effective interaction with $AlCl_4^-$. Consequently, the electrode demonstrated impressive long-cycle stability, retaining a capacity of 150 mAh g^{-1} after 13,000 cycles at 2 A g^{-1}[100]. Very recently Peng et al. established C = O groups COF supported by CNT, as cathode materials for Al-organic batteries (Fig. 9e)[101]. Aluminum batteries demonstrate a specific capacity of 290 mAh g^{-1} at 0.2 A g^{-1} and retain a reversible capacity of 170 mAh g^{-1} after 32,000 cycles at 10 A g—^{1}, achieving an energy density of 389 Wh kg—^{1} (Fig. 9f). This performance benefits from abundant C=O and C-N groups, which enable the storage of multiple $AlCl^{2}$ ions through a pseudocapacitive process. Additionally, the COF network and conductive CNT channels work synergistically to enhance structural stability and accelerate ion and electron diffusion. Together, these factors contribute to the impressive efficiency and longevity of aluminum batteries[98].

Wang et al. introduced an environmentally benign, low-cost, and sustainable COF that combines benzene and triazine rings for Mg^{2+} storage in cathodes[65]. Owing to abundant triazine rings, each COF repetitive unit can reversibly bond with 9 Mg^{2+} during the charge/discharge process (Fig. 9g). The COF-based cathode delivers high-rate capability at the current density ranging from 0.2C to 20C, with a capacity retention of 52% at 20 C. This triazine-based COF electrode demonstrated excellent long-term stability and an ultra-low-capacity decay rate of 0.0196% across 3000 cycles at a high rate of 5C (Fig. 9h). The interaction between the nitrogen atom's lone pair electrons in the triazine ring and the dipole-quadrupole effect improved the electronic conductivity of the COF material. The triazine rings acted as redox centers, showcasing excellent reaction kinetics and stability. The electrochemical performance comparation of various cathode materials for the CIBs, AIBs, and MIBs is summarized in Table 4. In comparation with

Table 2 | Electrochemical performance comparation of cathode materials for SIBs and PIBs

Battery type/ Metal type	Materials	Building blocks	Active materials and cathode proportion	Initial capacity (CC/DC/CD)	Cycling stability (RC/CD/CN)	Voltage (V)	Ref.
SIBs	TAPB-NDA COF	1,3,5-tris(4-aminophenyl)benzene (TAPB) and 1,4,5,8-naphthalene tetracarboxylic dianhydride (NDA)	(COF: CNT = 2:1) with Super P, and CMC- SBR binder at a weight ratio of 75:15:10	–/136.7/ 0.025 A g^{-1}	–/0.3 A g^{-1}/1000	1.5–3.5	109
SIBs	Bipolar porous organic electrode (BPOE)	*p*-dicyanobenzene	active material (70 wt.%), carbon black (20 wt.%), and CMC (10 wt.%)	–/~120/0.1 A g^{-1}	–/1.0 A g^{-1}/7000	1.3–4.1	83
SIBs	TQBQ-COF	tetraminophenone (TABQ) and cyclohexanehexaone (CHHO)	50 wt% TQBQ-COF powders, 40 wt% Super P and 10 wt% PVDF	–/~300/0.1 A g^{-1}	213.6/ 1.0 A g^{-1}/1000	1.0–3.6	85
PIBs	PT-Si-COF-Co	$Pc(OH)_8Co$ and silica gel	60 wt% active materials, 30 wt% Super P and 10 wt % PVDF binder	–/386/40 mA g^{-1}	118/1 A g^{-1}/5000	0.005–3.0	66
PIBs	DAAQ-COF	2,6-diaminoanthraquinone (DAAQ) and 1,3,5-triformylphloroglucinol (TFP)	60 wt % Active material (DAAQ-COF: CNT = 2:1 first), 30 wt% CNT dispersion (the solid content of CNTs is 20 wt%), and 10 wt% PVDF	–/157.7/0.1 A g^{-1}	~130/0.5 A g^{-1}/500	0.8–2.8	80
PIBs	TCNQ-CTF	tetracyanoquinodimethane (TCNQ)	CTFs, acetylene black, PVDF with a mass ratio of 7:2:1	–/161/0.1 A g^{-1}	85/5 A g^{-1}/1000	1.0–3.9	110
PIBs	Poly (pentacenetetrone sulfide) (PPTS)	Chlorobenzene and pyromellitic dianhydride	PPTS with Super P and CMC of 5:4:1	–/~260/0.1 A g^{-1}	190/5 A g^{-1}/3000	0.1–3.2	111
PIBs	Perylene	Perylene-3,4,9,10-tetracarboxylic dianhydride (PTCDA)	Active materials with carbon black, and CMC at a weight ratio of 8:1:1	–/126/0.1 A g^{-1}	98/1 A g^{-1}/1000	–	112
SIBs	Inorganic	$NaFe_{0.2}Mn_{0.4}Ni_{0.4}O_2$	active material, acetylene black, and PVDF in a weight ratio of 75:15:10	–/133/0.05 C	130/0.05 C/30	2.0–4.3	113
PIBs	Inorganic	$K_3V_2(PO_4)_3$/C nanocomposites	active material, super-P, and PVDF in a weight ratio of 80: 10: 10	77/54/20 mA g^{-1}	52/20 mA g^{-1} /100	2.5–4.3	114

CC charge capacity (mAh g^{-1}), *DC* discharge capacity: (mAh g^{-1}), *CD* current density, *RC* reversible capacity: (mAh g^{-1}), *CN* cycle number.

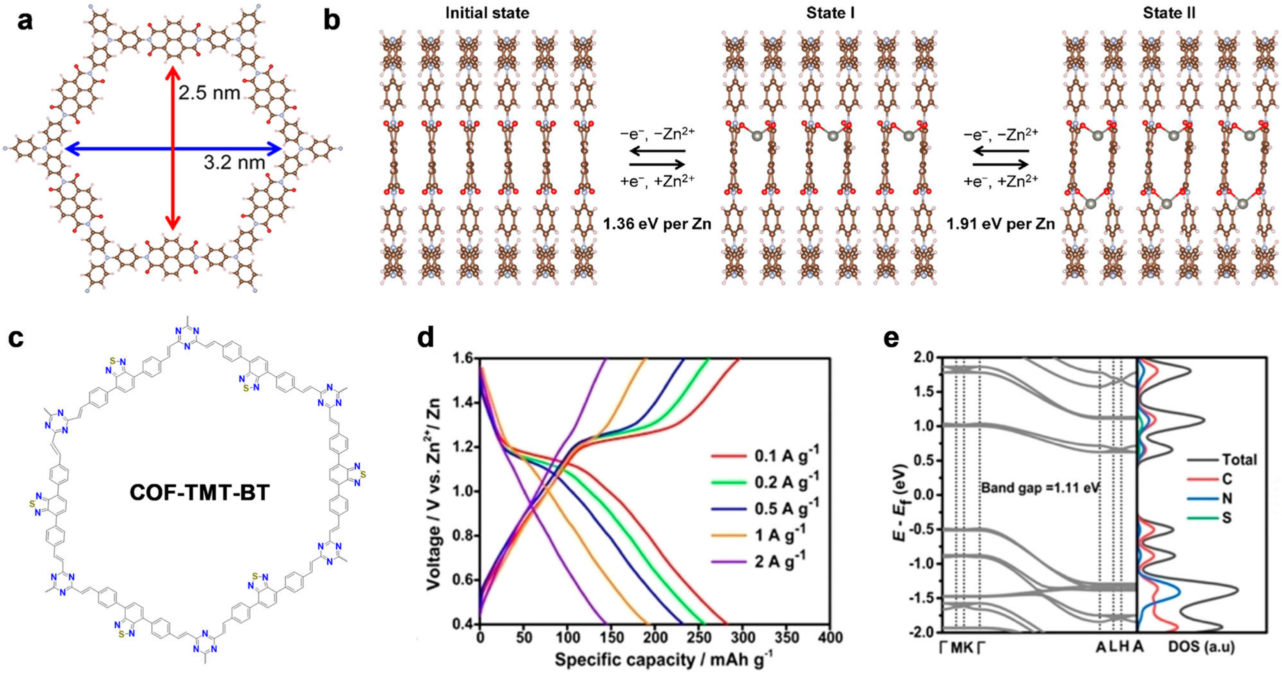

Fig. 8 | COF-based cathodes for ZIBs. a Structural representation of PI-COF. **b** Mechanistic analysis of Zn^{2+} storage. Reproduced with permission[90]. Copyright 2020, American Chemical Society. **c** Structural depiction of COF-TMT-BT. **d** Rate-dependent galvanostatic charge-discharge profiles of COF-TMT-BT electrodes. **e** Simulated density of states and band structures of COF-TMT-BT. Reproduced with permission[91]. Copyright 2023, Wiley-VCH.

inorganic cathodes, COF-based cathodes exhibit dramatically improved cycling performance and specific capacity.

Conclusion and outlook

This review provides a critical overview of the recent advancements of COFs beyond LIB technologies. COFs have emerged as promising cathodes for various battery systems, including SIBs, PIBs, ZIBs, CIBs, AIBs, and MIBs. Despite their potential, several critical factors influence their efficacy as cathodes. First, structural stability is paramount, as COFs must maintain their integrity during repeated charge-discharge cycles. Additionally, the presence of redox-active functional groups is essential for facilitating electron transfer and ion storage; the type and quantity of these redox sites significantly impact both capacity and rate performance. Furthermore, adequate electrical conductivity is crucial for efficient electron transport during charge-discharge cycles, which can be enhanced by incorporating conductive carbon substrates. The design of COFs must also consider pore size and structural configuration, which are vital for enabling efficient ion transport, especially for larger ions. Lastly, compatibility with the electrolyte employed in the battery is critical, necessitating stability in the presence of the electrolyte and facilitating ion transport. Based on these criteria, COFs exhibiting redox-active functional groups such as carbonyl (C=O) and imine (C=N), along with appropriate pore sizes, can serve effectively as cathodes. Based on the current research status, the prospects for future efforts on COF-based cathode in beyond-Li ion batteries are described as follows:

1. **Diversification of the redox monomers' scopes**. Exploring N-, P-, and bipolar organic electrode materials for HMIBs presents a promising avenue for enhancing energy storage technologies. N-type materials, like quinones and imides, could be optimized to improve their capacity and efficiency when paired with divalent cations. P-type materials may benefit from structural modifications to enhance their redox activity with multivalent anions, thereby increasing their specific capacity. Bipolar materials, capable of interacting with both cations and anions, offer unique advantages for utilizing the higher charge density of multivalent ions. Overall, focusing on these organic materials in multivalent ion battery systems could lead to next-generation batteries with improved efficiency and energy capacities.
2. **Improving the COFs electronic conductivity**. Among the class of COFs, to the best of our knowledge, the vinylene-linked COF (TFPPy-ICTO-COF) exhibits the highest conductivity reported to date, at $5.6 \times 10^{-3}\ \mathrm{S\ cm^{-1}}$[102]. The electronic conductivity of COFs plays a crucial role in the electrochemical performance of COF-based cathodes. Improving the intrinsic conductivity of COFs can significantly enhance their electrochemical performance while reducing the amount of conductive agents used and increasing the energy density of the system. Some strategies have been reported to improve the conductivity of COFs, such as enhancing the conjugation and heteroatom-doping, which are also promising for use in COF-based cathode optimization.
3. **Scale-up synthesis method**. The complex assembly of monomers has led to the diversity of COF types. However, the monomers, like 2,4,6-trimethyl-1,3,5-triazine (US$ 230 g^{-1})[103], 2,4,6-trimethylpyridine-3,5-dicarbonitrile (US$ 579 g^{-1})[104], 2,2',2''-(benzene-1,3,5-triyl)triacetonitrile (US$ 393 g^{-1})[105], and 2,2',6,6'-tetramethyl-4,4'-bipyridine (US$ 949 g^{-1})[106] are expensive, and often COF synthesis takes a prolonged reaction time (3–7 days) at high temperature, over 150 °C, which limits the large-scale production and industrial application of COFs. Therefore, designing COFs with low-cost monomers and catalysts and developing simple synthetic methods is another urgent problem to be solved.
4. **Mechanism investigation**. The investigation of mechanisms is essential for advancing COF-based cathodes as emerging materials. Specifically, the reaction mechanisms of these cathodes in various battery systems and their fading mechanisms require further exploration through advanced characterization techniques and theoretical calculations or simulations. Given their inherent instability under long-term, high-energy electron irradiation, cryo-TEM (transmission electron microscopy) is a valuable tool for studying COF-based cathodes, particularly in addressing interface chemistry and unveiling reaction principles and failure mechanisms. Additionally, in situ characterization techniques, such as Fourier transform infrared, Raman spectroscopy, and electrochemical impedance spectroscopy, are critical for the real-time detection of cathode reaction processes.

Table 3 | Electrochemical performance comparation of cathode materials for the ZIBs

Battery type/ Metal type	Materials	Building blocks	Active materials and cathode proportion	Initial capacity (CC/DC/CD)	Cycling stability (RC/CD/CN)	Voltage (V)	Ref.
ZIBs	HqTp-COF	2,5-diaminohydroquinone dihydrochloride (**Hq**) and 1,3,5-triformylphloroglucinol (**Tp**)	HqTp COF (4 mg) and pristine CNF (1 mg) in 3:1 water-IPA solution (1 ml), 5 wt% Nafion solution as binder	–/276/0.125 A g^{-1}	85/3.75 A g^{-1}/1000	0.2–1.8	115
ZIBs	HAQ-COF	1,2,4,5-tetramino-benzoquinone (**TABQ**) and hexaketocyclohexane octahydrate (**HKCO**)	COF powder, acetylene black carbon and PTFE (60 wt% dispersion in H_2O) of 6:3:1	–/344/0.1 A g^{-1}	128/5 A g^{-1}/10000	0.2–1.6	53
ZIBs	IISERP-COF22	2,4,6-triformylphenol and the protected ligand 3,4-bis((4-((E)- benzylideneamino)phenyl)amino)cyclobut-3-ene-1,2-dion	COF (50 mg; 80%), Super P carbon (15 mg; 15%), and 5% of Nafion binder (5 mg)	–/600/5 A g^{-1}	690/1.5 mA g^{-1}/6000	0.2–1.6	116
ZIBs	TfDa-COF	1,3,5-Triformylphloroglucinol (**TFP**), 2,6-diaminoanthraquinone **(DAAQ)**	COF, acetylene black and PVDF in a mass ratio of 7: 2: 1	–/72.5/0.2 A g^{-1}	96.6/0.1 A g^{-1} /10000	0.2–1.5	117
ZIBs	COF-TMT-BT	2,4,6-trimethyl-1,3,5-triazine (**TMT**) and 4,4'-(benzothiadiazole-4,7- diyl)dibenzaldehyde (**BT**)	70 wt% of COF-TMT-BT, 20 wt% of MWCNT, and 10 wt% of PTFE as the binder	–/146.2/2 A g^{-1}	283.5/0.1 A g^{-1}/2000	0.5–1.6	91
ZIBs	COF-PTO	1,3,5-triformylphloroglucinol (**TP**), 2,7-diaminopyrene-4,5,9,10-tetraone (**PTO-NH_2**)	COF-PTO (60 wt%), Keijen black (30 wt%), and PVDF (10 wt%)	–/96/15 A g^{-1}	105/10 A g^{-1}/18000	0.2–1.6	118
ZIBs	NT-COF	1,4,5,8-naphthalene tetracarboxylic dianhydride (**MTDA**) and tris (4-aminophenyl) amine (**TAPA**)	(NT-COF), acetylene black, and PTFE in a ratio of 5:4:1	–/214/0.2 A g^{-1}	143/1 A g^{-1}/800	0.2–1.6	119
ZIBs	DAAQ-COF	1,3,5- triformylphloroglucinol (**TFP**) and 2,6-diaminoanthraquinone (**DAAQ**)	DAAQ-COF, Acetylene Black, and PVDF in a 5: 4: 1	–/45/3 A g^{-1}	75/1 A g^{-1}/10000	0.2–1.4	120
ZIBs	p-chloranil	p-chloranil	p-chloranil with Super P carbon and CMC-SBR (in 2:1 ratio) in 60:35:5 weight ratio	–/170/43.4 mA g^{-1}	90/43.4 mA g^{-1}/100	0.8–1.4	121
ZIBs	quinone	calix[4]quinone (C4Q)	C4Q, Super P, and PVDF with weight ratio of 6:3.5:0.5.	–/335/0.02 A g^{-1}	215/0.5 A g^{-1}/100	0.2–1.8	88
ZIBs	Pyrene-4,5,9,10-tetraone (PTO)	Pyrene-4,5,9,10-tetraone (PTO)	Active material with Keijen black and PTFE in a mass ratio of 60:30:10	–/335/0.04 A g^{-1}	145/3 A g^{-1}/1000	0.36–1.46	122
ZIBs	Diquinoxalino [2,3-*a*:2′,3′-c] phenazine (HATN)	Hexaketocyclohexane octahydrate and o-phenylenediamine	HATN nanobelts, Super P and PVDF in a weight ratio of 6: 3.5 :0.5	–/225/0.1 A g^{-1}	140/5 A g^{-1}/5000	0.3–1.1	123
ZIBs	Thianthrene	thianthrene (TT)	active material, acetylene black and PVDF in a weight ratio of 7: 2: 1	–/112/0.5 A g^{-1}	~80/1 A g^{-1}/8000	0.8–1.7	124
ZIBs	inorganic	$Na_3V_2(PO_4)_2F_3$	70 wt% NVPF@C with 10 wt% acetylene black and 20 wt% PTFE	–/61.7/0.2 A g^{-1}	46/1 A g^{-1}/4000	0.8–1.9	125

CC charge capacity (mAh g^{-1}), *DC* discharge capacity: (mAh g^{-1}), *CD* current density, *RC* reversible capacity: (mAh g^{-1}), *CN* cycle number.

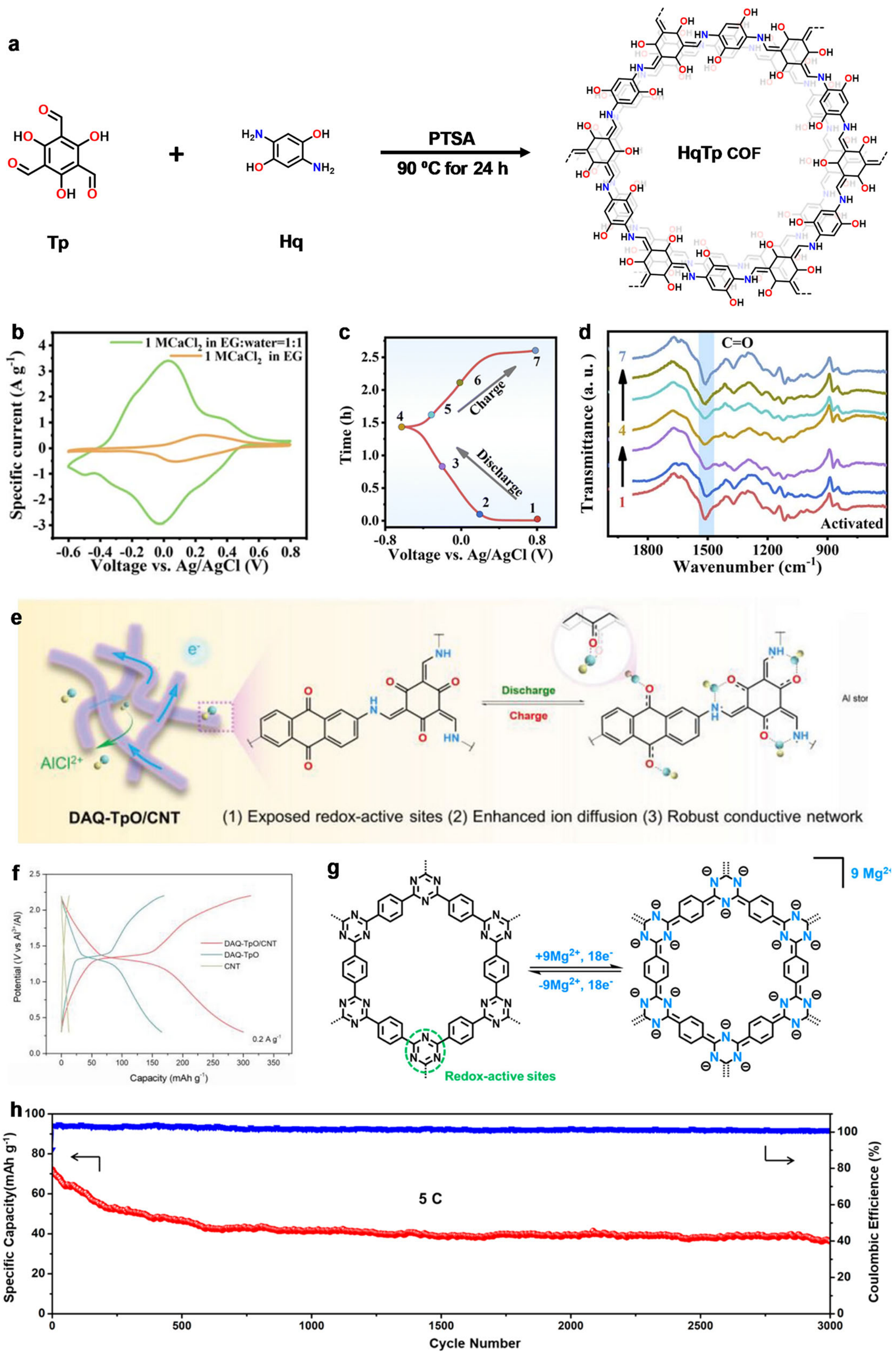

Fig. 9 | Performance and characterization of various COFs as cathodes in CIBs, AIBs, and MIBs. **a** Structure of HqTp COF. **b** CV curves analysis: Electrochemical behavior of the HqTp electrode in various electrolyte environments. **c** Galvanostatic charge-discharge profile of HqTp at 0.1 A g^{-1}. **d** Voltage-dependent FTIR spectra of HqTp. Reproduced with permission[98]. Copyright 2022, The Royal Society of Chemistry. **e** Schematic illustration of the DAQ-TpO/CNT multiple redox sites. **f** Galvanostatic discharge/charge profiles of DAQ-TpO/CNT, DAQ-TpO, and CNT at 0.2 A g^{-1}. Reproduced with permission[101]. Copyright 2024, Wiley-VCH. **g** Structure and reaction mechanism of the COF. **h** Cycling performance of the COF at 0.5C. Reproduced with permission[65]. Copyright 2020, American Chemical Society.

Table 4 | Electrochemical performance comparation of various cathode materials for CIBs, AIBs and MIBs

Battery type/ Metal type	Materials	Building blocks	Active materials and cathode proportion	Initial capacity (CC/DC/CD)	Cycling stability (RC/CD/CN)	Voltage (V)	Ref.
Calcium	HqTp-COF	2,5-diaminohydroquinone dihydrochloride (**Hq**) and 1,3,5-triformylphloroglucinol (**Tp**)	HqTp powder, Super p, and PVDF in a weight ratio of 4: 4: 2	–/91.4/1 A g^{-1}	63.2/3 A g^{-1}/1600	~0–1.7	98
AIBs	DAQ-TpOMe (DATP) COFs	2,6-diaminoanthraquinone (**DAQ**) and 2,4,6-Trimethoxy-benzene-1,3,5-tricarbaldehyde (**TpOMe**)	(60%COF + 40%CNT), with Keijen black and CMC at a weight ratio of 6:3:1	–/140/1 A g^{-1}	~100/ 2 A g^{-1}/10000	0.3–2.2	126
AIBs	DAQ-TpO COFs	2,6-Diaminoanthraquinone (**DAQ**), 1,3,5-triformylphloroglucinol (**TPO**)	(COF: CNT = ~ 80:20): Keijen black and CMC at a weight ratio of 6:3:1	–/290/0.2 A g^{-1}	170/ 10 A g^{-1}/32000	0.3–2.2	101
AIBs	2D-NT-COF	4′,4′′-(1,3,5-triazine-2,4,6-triyl) trainline (**TTTA**) and pyromellitic dianhydride (**PMDA**)	(COF: CNT = 70:30), Super P, and PVDF in the weight ratio of 7:2:1	–/132/0.1 A g^{-1}	~80/1 A g^{-1}/4000	–	96
MIBs	COF-N	tris(4-aminophenyl) amine (**TAPA**) and naphthalenetetracarboxylic dianhydride (**NTCDA**)	COFs (60%) and conductive carbon (30%), and PVDF (10%)	–/120/50 mA g^{-1}	108/0.2 A g^{-1}/300	0.2–2.5	127
AIBs	Phenanthrenequinone (**PQ**)-based compounds	PQ triangle (**PQ-Δ**)	PQ derivatives, Denka black, and PVDF (Arkema) binder in a weight ratio of 3:5:2	–/110/0.1 A g^{-1}	94/2 A g^{-1}/5000	0.7–2.35	128
AIBs	Heterocyclic quinone polymer	tetraaminobenzoquinone (TABQ) and pyrene-4,5,9,10-tetraone (PYT)	Active material (PYTQ: CNT = 2:1), with Keijen Black and carboxyl methylcellulose at a weight ratio of 6:3:1	–/295/0.1 A g^{-1}	85/1 A g^{-1}/4000	0.2–2.1	129
CIBs	Quinone	9,10-phenanthrenequinone (**PQ**)	PQ powder, SWCNTs, and PTFE in a weight ratio of 6:3:1	–/261.4/0.1 C	250/0.2 C/200	0.5–3.5	130
CIBs	triphenylamine	Polytriphenylamine (**PTPAn**)	60% PTPAn powder, 30% acetylene blacks and 10% PVDF	–/88/0.1 A g^{-1}	44/2 A g^{-1}/2000	–	131
CIBs	inorganic	NASCION-type N_1VPF_3	70 wt% $Na_3V_2(PO_4)_2F_3$, 20 wt% super P carbon, and 10 wt% PVDF	–/106/10 mA g^{-1}	–	1.5–4.5	132
MIBs	inorganic	Layered TiS_2	Layered TiS_2 with Super P and PVDF in 8:1:1 weight ratio	–/270/0.05 C at 60 °C	–	–	133

CC charge capacity (mAh g^{-1}), *DC* discharge capacity: (mAh g^{-1}), *CD* current density, *RC* reversible capacity: (mAh g^{-1}), *CN* cycle number.

These methods facilitate a comprehensive analysis of the reactions and their impact on electrochemical performance. As a result, the insights gained from these investigations can guide further improvements to COF-based cathodes, ultimately enhancing their functionality and longevity.

In summary, based on mechanistic insights, rational structural design can enhance the intrinsic electronic conductivity of COFs, reducing the proportion of conductive additives and thereby improving both the volumetric and gravimetric energy densities of COF-based cathodes. Concurrently, the development of green and efficient synthesis methods utilizing low-cost monomers will significantly advance the industrialization of COF materials.

Received: 26 November 2024; Accepted: 10 April 2025;

References

1. Carley, S. & Konisky, D. M. The justice and equity implications of the clean energy transition. *Nat. Energy* **5**, 569–577 (2020).
2. Ding, Y., Cai, P. & Wen, Z. Electrochemical neutralization energy: from concept to devices. *Chem. Soc. Rev.* **50**, 1495–1511 (2021).
3. Peng, C. et al. Recent progress of promising cathode candidates for sodium-ion batteries: current issues, strategy, challenge, and prospects. *Small Struct.* **4**, 2300150 (2023).
4. Risacher, F. & Fritz, B. Origin of salts and brine evolution of Bolivian and Chilean salars. *Aquat. Geochem* **15**, 123–157 (2009).
5. Duan, L. et al. A P_2/P_3 biphasic layered oxide composite as a high-energy and long-cycle-life cathode for potassium-ion batteries. *Angew. Chem. Int. Ed.* **63**, e202400868 (2024).
6. Sada, K., Darga, J. & Manthiram, A. Challenges and prospects of sodium-ion and potassium-ion batteries for mass production. *Adv. Energy Mater.* **13**, 2302321 (2023).
7. Guo, D., Chu, S., Zhang, B. & Li, Z. The Development and prospect of stable polyanion compound cathodes in LIBs and promising complementers. *Small Methods* **8**, 2400587 (2024).
8. Huang, H. et al. Polyanionic cathode materials: a comparison between Na-ion and K-ion batteries. *Adv. Energy Mater.* **14**, 2304251 (2024).
9. Shi, Y. et al. Ambient synthesis of vanadium-based Prussian blue analogues nanocubes for high-performance and durable aqueous zinc-ion batteries with eutectic electrolytes. *Angew. Chem. Int. Ed.* **63**, e202411579 (2024).
10. Du, K. et al. High-entropy Prussian blue analogues enable lattice respiration for ultrastable aqueous aluminum-ion batteries. *Adv. Mater.* **36**, 2404172 (2024).
11. Ge, Y. et al. Layered organic molecular crystal with one-dimensional ion migration channel for durable magnesium-based dual-ion batteries. *ACS Energy Lett.* **10**, 1615–1622 (2025).
12. Su, J. et al. Synergistic π-vonjugation organic cathode for ultra-stable aqueous aluminum batteries. *Small* **20**, 2312086 (2024).
13. Li, M. et al. Design strategies for nonaqueous multivalent-ion and monovalent-ion battery anodes. *Nat. Rev. Mater.* **5**, 276–294 (2020).
14. Chen, Y., Fan, K., Gao, Y. & Wang, C. Challenges and perspectives of organic multivalent metal-ion batteries. *Adv. Mater.* **34**, 2200662 (2022).
15. Pau, P. C. F., Berg, J. & McMillan, W. Application of Stokes' law to ions in aqueous solution. *J. Phys. Chem.* **94**, 2671–2679 (1990).
16. Hu, H. et al. Achieving reversible Mn^{2+}/Mn^{4+} double redox couple through anionic substitution in a P2-type layered oxide cathode. *Nano Energy* **99**, 107390 (2022).
17. Kim, Y. et al. Corrosion as the origin of limited lifetime of vanadium oxide-based aqueous zinc ion batteries. *Nat. Commun.* **13**, 2371 (2022).
18. Zhang, A. et al. Anhydride type film-forming electrolyte additives for high-temperature $LiNi_{0.6}Co_{0.2}Mn_{0.2}O_2$//graphite pouch cells. *Prog. Nat. Sci.* **33**, 320–327 (2023).
19. Wu, Y. et al. Nine-electron transfer of binder synergistic π-d conjugated coordination polymers as high-performance lithium storage materials. *Angew. Chem. Int. Ed.* **62**, e202215864 (2023).
20. Yang, Z., Wang, F., Meng, P., Luo, J. & Fu, C. Recent advances in developing organic positive electrode materials for rechargeable aluminum-ion batteries. *Energy Stor. Mater.* **51**, 63–79 (2022).
21. Poizot, P. et al. Opportunities and challenges for organic electrodes in electrochemical energy storage. *Chem. Rev.* **120**, 6490–6557 (2020).
22. Sun, T., Xie, J., Guo, W., Li, D. S. & Zhang, Q. Covalent–organic frameworks: advanced organic electrode materials for rechargeable batteries. *Adv. Energy Mater.* **10**, 1904199 (2020).
23. Zhu, L. et al. Chemical design of covalent organic frameworks for aqueous zinc batteries. *Energy Storage Mater.* **67**, 103297 (2024).
24. Li, Z., Fuhr, O., Fichtner, M. & Zhao-Karger, Z. Towards stable and efficient electrolytes for room-temperature rechargeable calcium batteries. *Energy Environ. Sci.* **12**, 3496–3501 (2019).
25. Kim, H. S. et al. Structure and compatibility of a magnesium electrolyte with a sulphur cathode. *Nat. Commun.* **2**, 427 (2011).
26. Sun, T. et al. A biodegradable polydopamine-derived electrode material for high-capacity and long-life lithium-ion and sodium-ion batteries. *Angew. Chem. Int. Ed.* **55**, 10662–10666 (2016).
27. Muench, S. et al. Polymer-based organic batteries. *Chem. Rev.* **116**, 9438–9484 (2016).
28. Li, Y. et al. High-energy-density quinone-based electrodes with $[Al(OTF)]^{2+}$ storage mechanism for rechargeable aqueous aluminum batteries. *Adv. Funct. Mater.* **31**, 2102063 (2021).
29. Cao, S., Zhang, H., Zhao, Y. & Zhao, Y. Pillararene/calixarene-based systems for battery and supercapacitor applications. *eScience* **1**, 28–43 (2021).
30. Song, Z. & Zhou, H. Towards sustainable and versatile energy storage devices: an overview of organic electrode materials. *Energy Environ. Sci.* **6**, 2280–2301 (2013).
31. Yang, Z. et al. Electrochemical energy storage for green grid. *Chem. Rev.* **111**, 3577–3613 (2011).
32. Ding, S.-Y. & Wang, W. Covalent organic frameworks (COFs): from design to applications. *Chem. Soc. Rev.* **42**, 548–568 (2013).
33. Diercks, C.S. & Yaghi, O.M. The atom, the molecule, and the covalent organic framework. *Science* **355** (2017).
34. Suleman, S. et al. Turning on singlet oxygen generation by outer-sphere microenvironment modulation in porphyrinic covalent organic frameworks for photocatalytic oxidation. *Angew. Chem. Int. Ed.* **63**, e202314988 (2024).
35. Suleman, S. et al. Regulating the generation of reactive oxygen species for photocatalytic oxidation by metalloporphyrinic covalent organic frameworks. *Chem. Eng. J.* **476**, 146623 (2023).
36. Yuan, Y. et al. Highly conductive imidazolate covalent organic frameworks with ether chains as solid electrolytes for lithium metal batteries. *Angew. Chem. Int. Ed.* **63**, e202402202 (2024).
37. Suleman, S. et al. Enhanced photocatalytic CO_2 reduction via linkage substitution in porphyrinic covalent organic frameworks. *CCS Chem.* **6**, 1689–1697 (2024).
38. Liu, X. et al. Gas-triggered gate-opening in a flexible three-dimensional covalent organic framework. *J. Am. Chem. Soc.* **146**, 11411–11417 (2024).
39. Tran, L. D. et al. Pore-wall decorated covalent organic frameworks for selective vapor sensing. *Adv. Funct. Mater.* 2402208 (2024).
40. Zhang, H. et al. Assembly-dissociation-reconstruction synthesis of covalent organic framework membranes with high continuity for efficient CO_2 separation. *Angew. Chem. Int. Ed.* e202411724 (2024).

41. Jin, E. et al. Two-dimensional sp^2 carbon–conjugated covalent organic frameworks. *Science* **357**, 673–676 (2017).
42. Li, C. et al. Anthraquinone-based silicate covalent organic frameworks as solid electrolyte interphase for high-performance lithium–metal batteries. *J. Am. Chem. Soc.* **145**, 24603–24614 (2023).
43. Liang, X., Tian, Y., Yuan, Y. & Kim, Y. Ionic covalent organic frameworks for energy devices. *Adv. Mater.* **33**, 2105647 (2021).
44. Wang, R. et al. Highly conductive covalent–organic framework films. *Small* **20**, 2306634 (2024).
45. Guan, L., Zou, J., Mao, M. & Wang, C. Constructing chelation for boosting storage of large-sized or multivalent ions. *Acc. Mater. Res.* **5**, 560–570 (2024).
46. Ke, S. W. et al. Integrating multiple redox-active units into conductive covalent organic frameworks for high-performance sodium-ion batteries. *Angew. Chem. Int. Ed.* **64**, e202417493 (2025).
47. Niu, C., Luo, W., Dai, C., Yu, C. & Xu, Y. High-voltage-tolerant covalent organic framework electrolyte with holistically oriented channels for solid-state lithium metal batteries with nickel-rich cathodes. *Angew. Chem. Int. Ed.* **60**, 24915–24923 (2021).
48. Li, Z. et al. Defective 2D covalent organic frameworks for postfunctionalization. *Adv. Funct. Mater.* **30**, 1909267 (2020).
49. Li, X. et al. Solution-processable covalent organic framework electrolytes for all-solid-state Li–organic batteries. *ACS Energy Lett.* **5**, 3498–3506 (2020).
50. Li, Z. et al. Cationic covalent organic framework based all-solid-state electrolytes. *Mater. Chem. Front.* **4**, 1164–1173 (2020).
51. Chen, H. et al. Cationic covalent organic framework nanosheets for fast Li-ion conduction. *J. Am. Chem. Soc.* **140**, 896–899 (2018).
52. Yang, X. et al. Mesoporous polyimide-linked covalent organic framework with multiple redox-active sites for high-performance cathodic Li storage. *Angew. Chem. Int. Ed.* **134**, e202207043 (2022).
53. Wang, W. et al. Molecular engineering of covalent organic framework cathodes for enhanced zinc-ion batteries. *Adv. Mater.* **33**, 2103617 (2021).
54. Yang, Z. et al. Surpassing the organic cathode performance for lithium-ion batteries with robust fluorinated covalent quinazoline networks. *ACS Energy Lett.* **6**, 41–51 (2020).
55. Zhang, Q. et al. Engineering covalent organic frameworks toward advanced zinc-based batteries. *Adv. Mater.* **36**, 2313152 (2024).
56. Ye, H. et al. Advanced covalent-organic framework materials for sodium-ion battery. *Prog. Nat. Sci.* **33**, 754–766 (2023).
57. Wang, C. et al. A pyrazine-pyridinamine covalent organic framework as a low potential anode for highly durable aqueous calcium-ion batteries. *Adv. Energy Mater.* **14**, 2302495 (2024).
58. Jindal, S. et al. p/n-type polyimide covalent organic frameworks for high-performance cathodes in sodium-ion batteries. *Small* 2407525 (2024).
59. Wen, F., Xu, K., Feng, Y. & Huang, N. Two-dimensional covalent organic frameworks with pentagonal pores. *J. Am. Chem. Soc.* **146**, 19680–19685 (2024).
60. Feng, X., Ding, X. & Jiang, D. Covalent organic frameworks. *Chem. Soc. Rev.* **41**, 6010–6022 (2012).
61. Yusran, Y., Guan, X., Li, H., Fang, Q. & Qiu, S. Postsynthetic functionalization of covalent organic frameworks. *Natl Sci. Rev.* **7**, 170–190 (2019).
62. Segura, J. L., Royuela, S. & Mar Ramos, M. Post-synthetic modification of covalent organic frameworks. *Chem. Soc. Rev.* **48**, 3903–3945 (2019).
63. Zheng, S. et al. Orthoquinone–based covalent organic frameworks with ordered channel structures for ultrahigh performance aqueous zinc–organic batteries. *Angew. Chem. Int. Ed.* **61**, e202117511 (2022).
64. Wang, S. et al. Exfoliation of covalent organic frameworks into few-layer redox-active nanosheets as cathode materials for lithium-ion batteries. *J. Am. Chem. Soc.* **139**, 4258–4261 (2017).
65. Sun, R. et al. A covalent organic framework for fast-charge and durable rechargeable Mg storage. *Nano Lett.* **20**, 3880–3888 (2020).
66. Liu, Z. et al. Unprecedented planar-square SiO_4-moiety connected two-dimensional covalent organic frameworks for anodic potassium ion storage. *CCS Chem*. **7**, 1–11 (2024).
67. Wang, C. et al. Recent progress in covalent organic frameworks for cathode materials. *Polymers* **16**, 687 (2024).
68. Haldar, S., Schneemann, A. & Kaskel, S. Covalent organic frameworks as model materials for fundamental and mechanistic understanding of organic battery design principles. *J. Am. Chem. Soc.* **145**, 13494–13513 (2023).
69. Wang, Z., Hu, J. & Lu, Z. Covalent organic frameworks as emerging battery materials. *Batteries Supercaps* **6**, e202200545 (2023).
70. Shehab, M. K., Weeraratne, K. S., Huang, T., Lao, K. U. & El-Kaderi, H. M. Exceptional sodium-ion storage by an aza-covalent organic framework for high energy and power density sodium-ion batteries. *ACS Appl. Mater. Interfaces* **13**, 15083–15091 (2021).
71. Tong, Z. et al. Ionic covalent organic frameworks with tailored anionic redox chemistry and selective ion transport for high-performance Na-ion cathodes. *J. Energy Chem.* **75**, 441–447 (2022).
72. Li, Z. et al. Synergistic effects between doped nitrogen and phosphorus in metal-free cathode for zinc-air battery from covalent organic frameworks coated CNT. *ACS Appl. Mater. Interfaces* **9**, 44519–44528 (2017).
73. Cheng, L. et al. Redox-bipolar covalent organic framework cathode for advanced sodium-organic batteries. *Adv. Mater.* **37**, 2411625 (2025).
74. Ma, D. et al. A carbonyl-rich covalent organic framework as a high-performance cathode material for aqueous rechargeable zinc-ion batteries. *Chem. Sci.* **13**, 2385–2390 (2022).
75. Yang, Z. et al. Intermolecular hydrogen bonding networks stabilized organic supramolecular cathode for ultra-high capacity and ultra-long cycle life rechargeable aluminum batteries. *Angew. Chem. Int. Ed.* **63**, e202403424 (2024).
76. Chen, X.-L. et al. Multiple accessible redox-active sites in a robust covalent organic framework for high-performance potassium storage. *J. Am. Chem. Soc.* **145**, 5105–5113 (2023).
77. DeBlase, C. R. et al. Rapid and efficient redox processes within 2D covalent organic framework thin films. *ACS Nano* **9**, 3178–3183 (2015).
78. Niu, L. et al. Production of two-dimensional nanomaterials via liquid-based direct exfoliation. *Small* **12**, 272–293 (2016).
79. Yuan, W. et al. Novel covalent organic framework/carbon nanotube composites with multiple redox-active sites for high-performance Na storage. *Energy Storage Mater.* **65**, 103142 (2024).
80. Duan, J. et al. Construction of a few-layered COF@CNT composite as an ultrahigh rate cathode for low-cost K-ion batteries. *ACS Appl. Mater. Interfaces* **14**, 31234–31244 (2022).
81. Zhao, Q., Lu, Y. & Chen, J. Advanced organic electrode materials for rechargeable sodium-ion batteries. *Adv. Energy Mater.* **7**, 1601792 (2017).
82. Zhang, Z. et al. Size effects in sodium ion batteries. *Adv. Funct. Mater.* **31**, 2106047 (2021).
83. Sakaushi, K. et al. Aromatic porous-honeycomb electrodes for a sodium-organic energy storage device. *Nat. Commun.* **4**, 1485 (2013).
84. Kim, M.-S., Lee, W.-J., Paek, S.-M. & Park, J. K. Covalent organic nanosheets as effective sodium-ion storage materials. *ACS Appl. Mater. Interfaces* **10**, 32102–32111 (2018).
85. Shi, R. et al. Nitrogen-rich covalent organic frameworks with multiple carbonyls for high-performance sodium batteries. *Nat. Commun.* **11**, 178 (2020).

86. Xu, Y. S. et al. High-performance cathode materials for potassium-ion batteries: structural design and electrochemical properties. *Adv. Mater.* **33**, 2100409 (2021).
87. Fang, G., Zhou, J., Pan, A. & Liang, S. Recent advances in aqueous zinc-ion batteries. *ACS Energy Lett.* **3**, 2480–2501 (2018).
88. Zhao, Q. et al. High-capacity aqueous zinc batteries using sustainable quinone electrodes. *Sci. Adv.* **4**, eaao1761 (2018).
89. Parker, J. F. et al. Rechargeable nickel–3D zinc batteries: an energy-dense, safer alternative to lithium-ion. *Science* **356**, 415–418 (2017).
90. Yu, M. et al. A high-rate two-dimensional polyarylimide covalent organic framework anode for aqueous Zn-ion energy storage devices. *J. Am. Chem. Soc.* **142**, 19570–19578 (2020).
91. Peng, H. et al. Supramolecular engineering of cathode materials for aqueous Zinc-ion energy storage devices: novel benzothiadiazole functionalized two-dimensional olefin-linked COFs. *Angew. Chem. Int. Ed.* **62**, e202216136 (2023).
92. Gummow, R. J., Vamvounis, G., Kannan, M. B. & He, Y. Calcium-ion batteries: current state-of-the-art and future perspectives. *Adv. Mater.* **30**, 1801702 (2018).
93. Das, S. K., Mahapatra, S. & Lahan, H. Aluminium-ion batteries: developments and challenges. *J. Mater. Chem. A* **5**, 6347–6367 (2017).
94. Das, A. et al. Prospects for magnesium ion batteries: a comprehensive materials review. *Coord. Chem. Rev.* **502**, 215593 (2024).
95. Zhang, S. et al. Covalent organic framework with multiple redox active sites for high-performance aqueous calcium ion batteries. *J. Am. Chem. Soc.* **145**, 17309–17320 (2023).
96. Liu, Y. et al. Redox-bipolar polyimide two-dimensional covalent organic framework cathodes for durable aluminium batteries. *Angew. Chem. Int. Ed.* **62**, e202306091 (2023).
97. Pallasch, S. M. et al. Porous azatruxene covalent organic frameworks for anion insertion in battery cells. *J. Am. Chem. Soc.* **146**, 17318–17324 (2024).
98. Li, L. et al. A covalent organic framework for high-rate aqueous calcium-ion batteries. *J. Mater. Chem. A* **10**, 20827–20836 (2022).
99. Leung, O. M., Schoetz, T., Prodromakis, T. & Ponce de Leon, C. Review—progress in electrolytes for rechargeable aluminium batteries. *J. Electrochem. Soc.* **168**, 056509 (2021).
100. Lu, H. et al. Two-dimensional covalent organic frameworks with enhanced aluminum storage properties. *ChemSusChem* **13**, 3447–3454 (2020).
101. Peng, X. et al. Boosting Aluminum storage in highly stable covalent organic frameworks with abundant accessible carbonyl groups. *Adv. Energy Mater*. **14**, 2400147 (2024).
102. Xu, X. et al. Janus dione-based conjugated covalent organic frameworks with high Conductivity as superior cathode materials. *J. Am. Chem. Soc.* **145**, 1022–1030 (2023).
103. Lyu, H., Diercks, C. S., Zhu, C. & Yaghi, O. M. Porous crystalline olefin-linked covalent organic frameworks. *J. Am. Chem. Soc.* **141**, 6848–6852 (2019).
104. Zhang, M. et al. Relative local electron density tuning in metal-covalent organic frameworks for boosting CO_2 photoreduction. *Angew. Chem. Int. Ed.* **62**, e202311999 (2023).
105. Cui, W.-R. et al. Regenerable and stable sp 2 carbon-conjugated covalent organic frameworks for selective detection and extraction of uranium. *Nat. Commun.* **11**, 436 (2020).
106. Bi, S., Meng, F., Wu, D. & Zhang, F. Synthesis of vinylene-linked covalent organic frameworks by monomer self-catalyzed activation of knoevenagel condensation. *J. Am. Chem. Soc.* **144**, 3653–3659 (2022).
107. Aziam, H. et al. Solid-state electrolytes for beyond lithium-ion batteries: a review. *Renew. Sust. Energ. Rev.* **167**, 112694 (2022).
108. Chen, L., An, Q. & Mai, L. Recent advances and prospects of cathode materials for rechargeable aqueous zinc-ion batteries. *Adv. Mater. Interfaces* **6**, 1900387 (2019).
109. Biswas, S. et al. 2D covalent organic framework covalently anchored with carbon nanotube as high-performance cathodes for lithium and sodium-ion batteries. *Small* **20**, 2406173 (2024).
110. Yang, H. et al. Polar covalent triazine frameworks as high-performance potassium metal battery cathodes. *Small* **20**, 2406737 (2024).
111. Tang, M. et al. An organic cathode with high capacities for fast-charge potassium-ion batteries. *J. Mater. Chem. A* **7**, 486–492 (2019).
112. Fan, L., Ma, R., Wang, J., Yang, H. & Lu, B. An ultrafast and highly stable potassium–organic battery. *Adv. Mater.* **30**, 1805486 (2018).
113. Yuan, D. D., Wang, Y. X., Cao, Y. L., Ai, X. P. & Yang, H. X. Improved electrochemical performance of Fe-substituted $NaNi_{0.5}Mn_{0.5}O_2$ cathode materials for sodium-ion batteries. *ACS Appl. Mater. Interfaces* **7**, 8585–8591 (2015).
114. Han, J. et al. Investigation of $K_3V_2(PO_4)_3$/C nanocomposites as high-potential cathode materials for potassium-ion batteries. *Chem. Commun.* **53**, 1805–1808 (2017).
115. Khayum, M. A. et al. Zinc ion interactions in a two-dimensional covalent organic framework based aqueous zinc ion battery. *Chem. Sci.* **10**, 8889–8894 (2019).
116. Kushwaha, R. et al. Made to measure squaramide COF cathode for zinc dual-ion battery with enriched storage via redox electrolyte. *Adv. Energy Mater.* **13**, 2301049 (2023).
117. Li, L. et al. An anthraquinone-based covalent organic framework for highly reversible aqueous zinc-ion battery cathodes. *J. Mater. Chem. A* **11**, 26221–26229 (2023).
118. Zhong, L. et al. Self-charging aqueous Zn//COF battery with ultra high self-charging efficiency and rate. *Adv. Mater.* **36**, 2314050 (2024).
119. Wang, S. et al. High-performance aqueous zinc-organic battery with a photo-responsive covalent organic framework cathode. *Small Methods* 2400557 (2024).
120. Wei, Y. et al. The compatibility of COFs cathode and optimized electrolyte for ultra-long lifetime rechargeable aqueous zinc-ion battery. *ChemSusChem* **17**, e202301851 (2024).
121. Kundu, D. et al. Organic cathode for aqueous Zn-ion batteries: taming a unique phase evolution toward stable electrochemical cycling. *Chem. Mater.* **30**, 3874–3881 (2018).
122. Guo, Z. et al. An environmentally friendly and flexible aqueous zinc battery using an organic cathode. *Angew. Chem. Int. Ed.* **130**, 11911–11915 (2018).
123. Tie, Z., Liu, L., Deng, S., Zhao, D. & Niu, Z. Proton insertion chemistry of a zinc–organic battery. *Angew. Chem. Int. Ed.* **59**, 4920–4924 (2020).
124. Cui, H. et al. High-voltage organic cathodes for zinc-ion batteries through electron cloud and solvation structure regulation. *Angew. Chem. Int. Ed.* **61**, e202203453 (2022).
125. Li, W., Wang, K., Cheng, S. & Jiang, K. A long-life aqueous Zn-ion battery based on $Na_3V_2(PO_4)_2F_3$ cathode. *Energy Storage Mater.* **15**, 14–21 (2018).
126. Peng, X. et al. Multi-redox covalent organic frameworks for aluminium organic batteries. *Energy Storage Mater.* **71**, 103674 (2024).
127. Gui, H. & Xu, F. Covalent organic framework cathodes for rechargeable Mg batteries. *Mater. Lett.* **346**, 134549 (2023).
128. Kim, D. J. et al. Rechargeable aluminium organic batteries. *Nat. Energy* **4**, 51–59 (2019).
129. Peng, X. et al. Heterocyclic conjugated polymer nanoarchitectonics with synergistic redox-active sites for high-performance aluminium organic batteries. *Angew. Chem. Int. Ed.* **134**, e202203646 (2022).
130. Ma, Y. et al. A small molecular cathode for high-performance calcium metal batteries. *Adv. Funct. Mater.* **35**, 2411715 (2025).
131. Zhou, R. et al. An advanced organic cathode for non-aqueous and aqueous calcium-based dual ion batteries. *J. Power Sources* **569**, 232995 (2023).

132. Chen, C., Shi, F., Zhang, S., Su, Y. & Xu, Z.-L. Ultrastable and high energy calcium rechargeable batteries enabled by calcium intercalation in a NASICON cathode. *Small* **18**, 2107853 (2022).
133. Sun, X., Bonnick, P. & Nazar, L. F. Layered TiS_2 positive electrode for Mg batteries. *ACS Energy Lett.* **1**, 297–301 (2016).
134. Lin, Z. et al. An anti-aromatic covalent organic framework cathode with dual-redox centers for rechargeable aqueous zinc batteries. *ACS Appl. Mater. Interfaces* **14**, 38689–38695 (2022).
135. Wang, Y., Wang, X., Tang, J. & Tang, W. A quinoxalinophenazinedione covalent triazine framework for boosted high-performance aqueous zinc-ion batteries. *J. Mater. Chem. A* **10**, 13868–13875 (2022).
136. Li, S. et al. A stable covalent organic framework cathode enables ultra-long cycle life for alkali and multivalent metal rechargeable batteries. *Energy Storage Mater.* **48**, 439–446 (2022).
137. Zou, G. et al. A Symmetric aqueous magnesium ion supercapattery based on covalent organic frameworks. *Adv. Energy Mater.* **13**, 2203193 (2023).

Acknowledgements

This work was supported by the Research Grants Council of the Hong Kong SAR Government (General Research Fund, #16306921 and #16306022; Collaborative Research Fund, #C6047-23GF), Innovation and Technology Support Programme (ITS/077/23), Green Tech Fund (GTF202220159), and HKUST-POSTECH Joint Research Seed Grant Program & Global Knowledge Network Awards.

Author contributions

S.S. and X.C. contributed equally to this work. S.S. and X.C. contributed to writing, revising, and editing. M.G. contributed to tabulation and revision. Y.K. supervised and directed this project. All authors discussed the results and commented on the manuscript.

Competing interests

The authors declare no competing interests.

Additional information

Supplementary information The online version contains supplementary material available at https://doi.org/10.1038/s43246-025-00801-7.

Correspondence and requests for materials should be addressed to Yoonseob Kim.

Peer review information *Communications Materials* thanks Rahul Banerjee and the other, anonymous, reviewer(s) for their contribution to the peer review of this work. Primary Handling Editors: Jet-Sing Lee. [A peer review file is available].

Reprints and permissions information is available at http://www.nature.com/reprints